severity. *Gastroenterology.* 1999;116(6):1413–1419.
38. Horton JD, et al. Combined analysis of oligonucleotide microarray data from transgenic and knockout mice identifies direct SREBP target genes. *Proc Natl Acad Sci U S A.* 2003;100(21):12027–12032.
39. Kim BJ, Fulton AB. The genetics and ocular findings of Alagille syndrome. *Semin Ophthalmol.* 2007;22(4):205–210.
40. Loomes KM, et al. Bile duct proliferation in liver-specific Jag1 conditional knockout mice: effects of gene dosage. *Hepatology.* 2007;45(2):323–330.
41. Nishikawa Y, et al. Transdifferentiation of mature rat hepatocytes into bile duct-like cells in vitro. *Am J Pathol.* 2005;166(4):1077–1088.
42. McCright B, Lozier J, Gridley T. A mouse model of Alagille syndrome: Notch2 as a genetic modifier of Jag1 haploinsufficiency. *Development.* 2002;129(4):1075–1082.
43. McDaniell R, et al. NOTCH2 mutations cause Alagille syndrome, a heterogeneous disorder of the notch signaling pathway. *Am J Hum Genet.* 2006; 79(1):169–173.
44. Kodama Y, Hijikata M, Kageyama R, Shimotohno K, Chiba T. The role of notch signaling in the development of intrahepatic bile ducts. *Gastroenterology.* 2004;127(6):1775–1786.
45. Suzuki A, et al. Flow-cytometric separation and enrichment of hepatic progenitor cells in the developing mouse liver. *Hepatology.* 2000;32(6):1230–1239.
46. Leclercq IA, Farrell GC, Schriemer R, Robertson GR. Leptin is essential for the hepatic fibrogenic response to chronic liver injury. *J Hepatol.* 2002;37(2):206–213.
47. Sahai A, et al. Obese and diabetic *db/db* mice develop marked liver fibrosis in a model of nonalcoholic steatohepatitis: role of short-form leptin receptors and osteopontin. *Am J Physiol Gastrointest Liver Physiol.* 2004;287(5):G1035–G1043.
48. Horie Y, et al. Hepatocyte-specific Pten deficiency results in steatohepatitis and hepatocellular carcinomas. *J Clin Invest.* 2004;113(12):1774–1783.
49. Luedde T, et al. Deletion of NEMO/IKKgamma in liver parenchymal cells causes steatohepatitis and hepatocellular carcinoma. *Cancer Cell.* 2007; 11(2):119–132.
50. Isoda K, et al. Deficiency of interleukin-1 receptor antagonist deteriorates fatty liver and cholesterol metabolism in hypercholesterolemic mice. *J Biol Chem.* 2005;280(8):7002–7009.
51. Nakanishi Y, et al. Nonalcoholic steatohepatitis and hepatocellular carcinoma in galectin-3 knockout mice. *Hepatol Res.* 2008;38(12):1241–1251.
52. Yanagitani A, et al. Retinoic acid receptor alpha dominant negative form causes steatohepatitis and liver tumors in transgenic mice. *Hepatology.* 2004;40(2):366–375.
53. Nakayama H, et al. Transgenic mice expressing nuclear sterol regulatory element-binding protein 1c in adipose tissue exhibit liver histology similar to nonalcoholic steatohepatitis. *Metabolism.* 2007;56(4):470–475.
54. Consortium ECTS. Identification and characterization of the tuberous sclerosis gene on chromosome 16. *Cell.* 1993;75(7):1305–1315.
55. van Slegtenhorst M, et al. Identification of the tuberous sclerosis gene TSC1 on chromosome 9q34. *Science.* 1997;277(5327):805–808.
56. Li Z, White P, Tuteja G, Rubins N, Sackett S, Kaestner KH. Foxa1 and Foxa2 regulate bile duct development in mice. *J Clin Invest.* 2009;119(6):1537–1545.
57. Kuhn R, Schwenk F, Aguet M, Rajewsky K. Inducible gene targeting in mice. *Science.* 1995; 269(5229):1427–1429.
58. Postic C, Magnuson MA. DNA excision in liver by an albumin-Cre transgene occurs progressively with age. *Genesis.* 2000;26(2):149–150.
59. Tanigaki K, et al. Regulation of alphabeta/gammadelta T cell lineage commitment and peripheral T cell responses by Notch/RBP-J signaling. *Immunity.* 2004;20(5):611–622.
60. de Alboran IM, et al. Analysis of C-MYC function in normal cells via conditional gene-targeted mutation. *Immunity.* 2001;14(1):45–55.
61. Kamura T, et al. Cytoplasmic ubiquitin ligase KPC regulates proteolysis of $p27^{Kip1}$ at G1 phase. *Nat Cell Biol.* 2004;6(12):1229–1235.
62. Nishiyama M, Nakayama K, Tsunematsu R, Tsukiyama T, Kikuchi A, Nakayama KI. Early embryonic death in mice lacking the beta-catenin-binding protein Duplin. *Mol Cell Biol.* 2004;24(19):8386–8394.
63. Morita S, Kojima T, Kitamura T. Plat-E: an efficient and stable system for transient packaging of retroviruses. *Gene Ther.* 2000;7(12):1063–1066.

Cell Stem Cell
Short Article

p57 Is Required for Quiescence and Maintenance of Adult Hematopoietic Stem Cells

Akinobu Matsumoto,[1,2] Shoichiro Takeishi,[1,2] Tomoharu Kanie,[1,2] Etsuo Susaki,[1,2] Ichiro Onoyama,[1,2] Yuki Tateishi,[1,2] Keiko Nakayama,[2,3] and Keiichi I. Nakayama[1,2,*]
[1]Department of Molecular and Cellular Biology, Medical Institute of Bioregulation, Kyushu University, 3-1-1 Maidashi, Higashi-ku, Fukuoka, Fukuoka 812-8582, Japan
[2]CREST, Japan Science and Technology Agency (JST), Kawaguchi, Saitama 332-0012, Japan
[3]Department of Developmental Genetics, Center for Translational and Advanced Animal Research, Graduate School of Medicine, Tohoku University, 2-1 Seiryo-machi, Aoba-ku, Sendai 980-8575, Japan
*Correspondence: nakayak1@bioreg.kyushu-u.ac.jp
DOI 10.1016/j.stem.2011.06.014

SUMMARY

Quiescence is required for the maintenance of hematopoietic stem cells (HSCs). Members of the Cip/Kip family of cyclin-dependent kinase (CDK) inhibitors (p21, p27, p57) have been implicated in HSC quiescence, but loss of p21 or p27 in mice affects HSC quiescence or functionality only under conditions of stress. Although p57 is the most abundant family member in quiescent HSCs, its role has remained uncharacterized. Here we show a severe defect in the self-renewal capacity of p57-deficient HSCs and a reduction of the proportion of the cells in G_0 phase. Additional ablation of p21 in a p57-null background resulted in a further decrease in the colony-forming activity of HSCs. Moreover, the HSC abnormalities of p57-deficient mice were corrected by knocking in the *p27* gene at the *p57* locus. Our results therefore suggest that, among Cip/Kip family CDK inhibitors, p57 plays a predominant role in the quiescence and maintenance of adult HSCs.

INTRODUCTION

Progression of the cell cycle is controlled by pairs of cyclins and cyclin-dependent kinases (CDKs). Progression through G_1 phase of the cell cycle is dependent on the cyclin D-CDK4 (or CDK6) complex, whereas cyclin E-CDK2 is required for the G_1-S transition and cyclins A and B together with CDK1 are required for G_2-M progression (Sherr and Roberts, 2004). Cell cycle progression is also under the control of negative regulators, the CDK inhibitors (CKIs), which belong to either the Ink4 or Cip/Kip families. Members of the Ink4 family—such as $p16^{Ink4a}$, $p15^{Ink4b}$, $p18^{Ink4c}$, and $p19^{Ink4d}$—are inhibitors specific for CDK4 or CDK6, whereas those of the Cip/Kip family, including $p21^{Cip1}$ (p21), $p27^{Kip1}$ (p27), and $p57^{Kip2}$ (p57), mainly target CDK2 and CDK4 (and CDK1 in some situations) for inhibition.

Sustained hematopoiesis in adults requires preservation of a quiescent, multipotential hematopoietic stem cell (HSC) pool that intermittently yields progenitors with robust proliferative potential (Arai and Suda, 2007). In contrast, the cell cycle of HSCs is active during embryogenesis in order to ensure expansion of the stem cell pool (Pawliuk et al., 1996). The ability of adult HSCs to reside in the quiescent state has been thought to be pivotal for maintenance of their "stemness." However, the precise mechanisms by which such quiescence is established, maintained, and terminated have been largely unknown. CKIs including p21, p27, and p57 are implicated in the maintenance of quiescence, given their function to antagonize CDK activity that promotes cell proliferation. However, self-renewal of HSCs in mice deficient in p21 was found to be impaired only under stressful conditions in which DNA is damaged by exposure to 5-fluorouracil or γ-irradiation (Cheng et al., 2000b; van Os et al., 2007). Deletion of p27 in mice also does not affect the number, cycling, or self-renewal of HSCs (Cheng et al., 2000a). Although many studies have suggested the importance of p57 for maintenance of HSC stemness (Miyamoto et al., 2007; Qian et al., 2007; Yamazaki et al., 2006), the role of p57 in control of HSC quiescence has remained poorly characterized. Unlike p21- or p27-deficient mice, mice lacking p57 die immediately after birth, manifesting severe developmental defects (Takahashi et al., 2000; Yan et al., 1997; Zhang et al., 1997), which has rendered functional characterization of their HSCs technically difficult.

We have now established mice in which the p57 gene is conditionally disrupted in the hematopoietic system in order to avoid the neonatal mortality of conventional p57-deficient mice. Deletion of p57 alone, but not that of p21 or p27, resulted in a reduction in HSC number, in the size of the G_0 population, and in their reconstitution ability after transplantation. Mice lacking both p21 and p57 showed a more severe phenotype than those lacking p57 alone, and knockin of the gene for p27 at the *p57* locus corrected the abnormalities of p57-deficient mice, suggestive of functional overlap between p57 and either p21 or p27. Our data thus indicate that p57 plays the dominant role among CKIs of the Cip/Kip family in maintenance of quiescence and stemness of HSCs.

RESULTS

p57 Is Predominantly Expressed in the Long-Term HSC Population

A previous study suggested that, among hematopoietic cells, p57 mRNA is most abundant in $CD34^-c\text{-}Kit^+Sca\text{-}1^+$ lineage marker-negative (Lin^-) HSCs ($CD34^-KSL$ HSCs), a fraction with

long-term repopulating capacity (Yamazaki et al., 2006). In contrast, p21 mRNA was not detected in $CD34^-KSL$ HSCs, whereas p27 mRNA was found to be present in both $CD34^-KSL$ and $CD34^+KSL$ cells, the latter corresponding to a fraction with short-term repopulating capacity. To examine the expression of p57 in HSCs at the protein level, we performed immunoblot analysis of sorted bone marrow (BM) samples from 12 wild-type mice at 8 weeks of age. We sorted and fractionated KSL cells with the SLAM (signaling lymphocytic activation molecule) marker CD150. Similar to the pattern observed for its mRNA, p57 protein was most abundant in the $CD150^+KSL$ fraction, a fraction with long-term repopulating capacity; it was present in smaller amounts in the $CD150^-KSL$ fraction, a fraction with short-term repopulating capacity, and it was not detected in other fractions (Figure 1A). We did not detect p21 in any of the fractions tested, whereas p27 was expressed at a low level in the $CD150^+KSL$ and $CD150^-KSL$ populations. These patterns of protein expression prompted us to examine the effects of p57 ablation in HSCs.

Deletion of p57 Leads to a Reduction in Size of the HSC Population

Given that most conventional p57 knockout mice die during the perinatal period as a result of respiratory distress, probably caused by skeletal anomalies (Takahashi et al., 2000; Yan et al., 1997; Zhang et al., 1997), it has been technically difficult to characterize adult HSCs in such mice. We therefore established mouse embryonic stem cells (ESCs) that harbor a "floxed" *p57* allele in which exons 2 to 4 (which include the entire coding region) are flanked by loxP sites (see Figure S1A available online). This allele was generated by homologous recombination followed by transient transfection of the ESCs with a vector for Cre recombinase in order to remove the introduced *neo* cassette (Figure S1B). Mice heterozygous for the floxed allele ($p57^{+/F}$ mice) were generated by microinjection of the mutant ESCs into blastocysts and breeding of the resultant chimeric animals with mice of the C57BL/6 strain. The *p57* locus undergoes genomic imprinting, with only the maternal allele being expressed (Matsuoka et al., 1995). The $p57^{+/F}$ mice were indistinguishable from wild-type animals, confirming that the floxed allele is functional. We also confirmed that the phenotype of mice in which the maternal floxed allele was deleted by Cre recombinase expressed from the EIIa gene promoter (Lakso et al., 1996) beginning early during embryogenesis was identical to that of conventional p57 knockout mice (Figure S1C). To ablate the maternal *p57* allele only in the hematopoietic system, we crossed female $p57^{+/F}$ mice with male mice harboring a Cre transgene under the control of the promoter for the myxovirus resistance 1 (Mx1) gene. We confirmed that almost all floxed alleles were inactivated by Cre recombinase in BM of Mx1-Cre/$p57^{+/F}$ mice after intraperitoneal injection of poly(I)-poly(C) [poly(I:C)] to activate the Mx1 gene promoter (Figure S1D). Without poly(I:C) injection, a slight decrease in the abundance of p57 mRNA was observed in Mx1-Cre/$p57^{+/F}$ mice compared with that in Mx1-Cre/$p57^{+/+}$ mice. Deletion of the *p57* allele resulted in a small increase in the amounts of p27 and p18 mRNAs in KSL cells, whereas deletion of p21 or p27 did not significantly affect the abundance of mRNAs for the corresponding other two CKIs (Figures S1E–S1H).

As early as 4 weeks after poly(I:C) injection, a substantial reduction in the size of the KSL fraction was apparent in p57-deficient mice compared with that in control littermates (Mx1-Cre/$p57^{+/+}$ mice), which were also injected with poly(I:C) to exclude the possibility that poly(I:C) affected phenotype regardless of genotype (Figure 1B). This reduction in the size of the KSL fraction in p57-deficient mice was apparent for all KSL subpopulations examined ($CD150^-$, $CD150^+CD48^-$, $CD34^-$, or $CD34^+$ cells) with the exception of $CD150^+CD48^+$ cells (Figure 1C). The total number and composition of cells in BM or peripheral blood were not otherwise affected by deletion of p57 at 4 weeks (Figures S1I–S1K and data not shown) or 4 months (Figure S1L and data not shown) after injection of poly(I:C), probably in part because the effect of such deletion in adult HSCs was compensated for at later stages of differentiation or had not had sufficient time to become manifest in the periphery within the period before analysis. In contrast, no reduction in the size of the HSC population was observed in p21- or p27-deficient mice (Figure 1C), consistent with the results of previous studies (Cheng et al., 2000a, 2000b; van Os et al., 2007). These findings thus suggested that p57 deletion affects the self-renewal capacity of HSCs.

Deletion of p57 Abrogates the Self-Renewal Capacity of HSCs

To assess the repopulating capacity of p57-deficient HSCs in vivo, we performed a competitive reconstitution assay in which BM cells (4×10^5) from poly(I:C)-injected Mx1-Cre/$p57^{+/+}$ or Mx1-Cre/$p57^{+/F}$ mice (CD45.2) competed against an equal number of BM cells from C57BL/6 heterozygous congenic mice (CD45.1/CD45.2) to reconstitute the hematopoietic compartment of irradiated C57BL/6 congenic mouse (CD45.1) recipients. At 16 weeks after BM cell transplantation (BMT), flow cytometric analysis of peripheral blood of the recipients revealed that the repopulating capacity of p57-deficient BM cells was markedly impaired, whereas that of $p21^{-/-}$ or $p27^{-/-}$ BM cells did not differ from that of cells from littermate controls (Figure 2A). Given that this result might have reflected the reduced number of HSCs in p57-deficient mice (Figures 1B and 1C), we also performed similar assays with total KSL cells (1.5×10^3) or $CD150^+CD48^-KSL$ cells (2.0×10^2) isolated from p57-deficient mice or littermate controls at 4 weeks after poly(I:C) injection. The p57-deficient KSL cells showed a greatly impaired repopulating capacity after the first BMT, and this impairment was even more pronounced after a second BMT (Figures 2B and 2C). In addition, the frequency of KSL cells derived from p57-deficient donors among BM cells of the recipient mice was markedly smaller than that for KSL cells derived from control donors (Figure 2D). To determine whether p57 intrinsically regulates HSC repopulating capability, we transplanted BM cells (4×10^5) from either Mx1-Cre/$p57^{+/F}$ mice or littermate controls not treated with poly(I:C) into lethally irradiated recipients together with the same number of competitor cells. After 4 weeks, we confirmed that donor cells were reconstituted in recipient BM and then injected the recipient mice with poly(I:C). Within 1 month after poly(I:C) injection, p57-deficient HSCs lost long-term repopulating capability and were eventually competed out by wild-type HSCs (Figure 2E), suggesting that a homing defect of transferred BM cells probably was not responsible for the impaired BM reconstitution by p57-deficient HSCs.

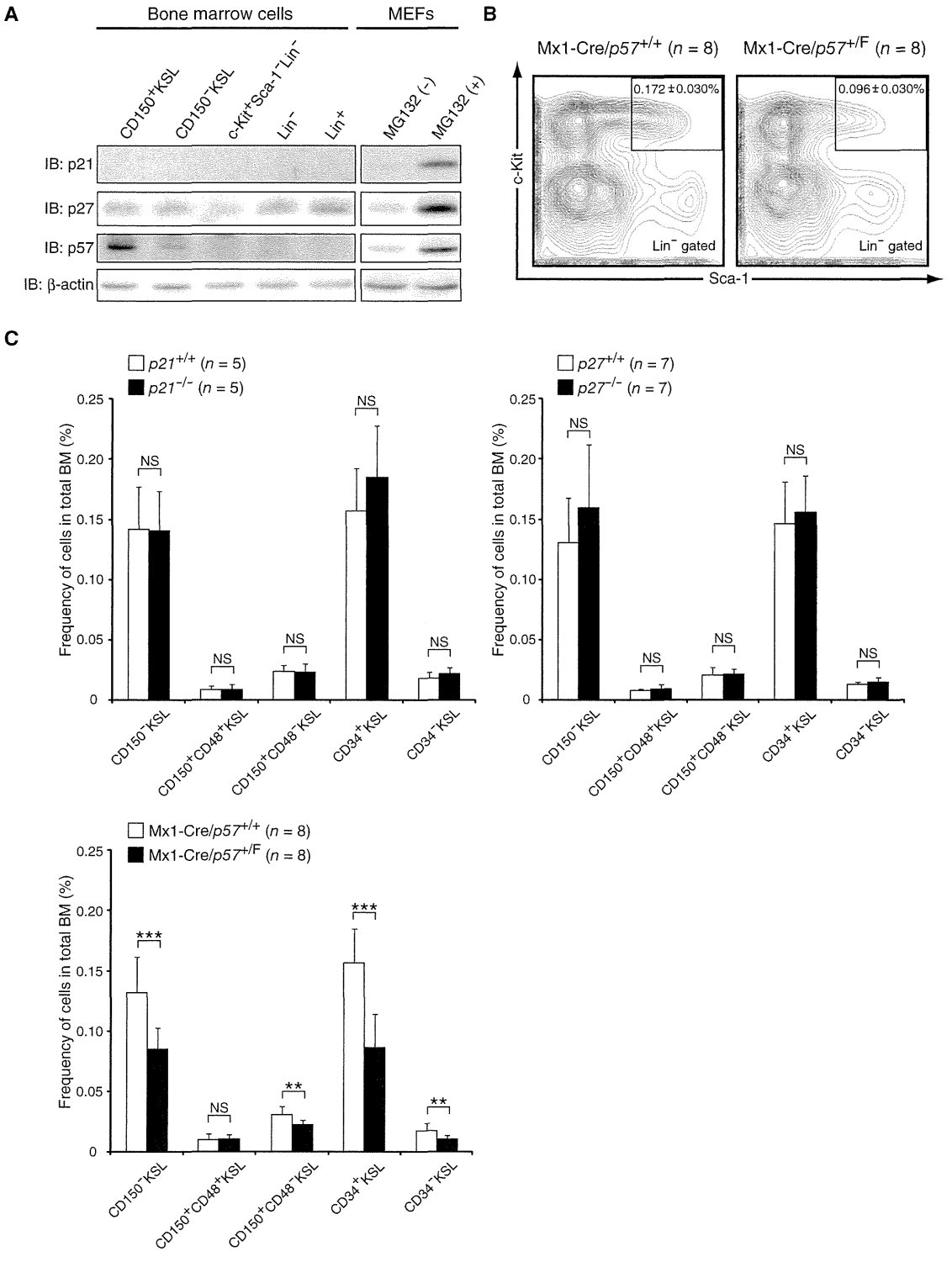

Figure 1. Decrease in HSC Number Induced by p57 Deletion

(A) Immunoblot analysis (IB) of fractionated hematopoietic cells from BM of wild-type mice. For positive and negative controls, mouse embryonic fibroblasts (MEFs) were cultured with or without 100 μM MG132, respectively.

(B) Flow cytometric determination of the frequency of KSL cells among BM cells of Mx1-Cre/$p57^{+/+}$ and Mx1-Cre/$p57^{+/F}$ mice at 4 weeks after poly(I:C) injection. The percentages of KSL cells among total BM cells are shown as means ± SD.

(C) Frequency of the indicated fractions among total BM cells from mice of the indicated genotypes. Mice harboring the Mx1-Cre transgene were examined at 4 weeks after poly(I:C) injection. Data are means ± SD. $^{**}p < 0.01$, $^{***}p < 0.005$; NS, not significant.

See also Figure S1.

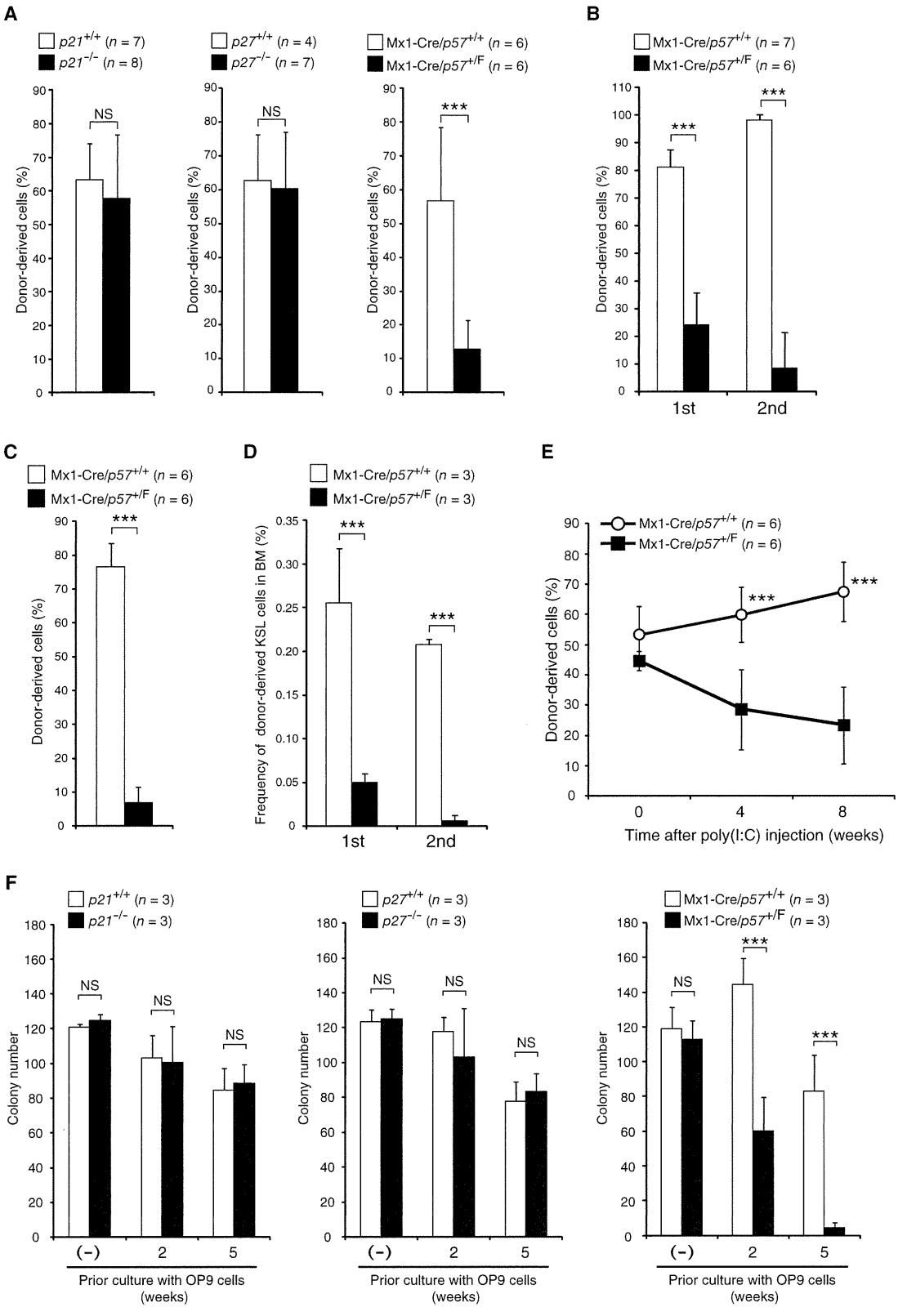

Figure 2. p57, but Not p21 or p27, Is Essential for HSC Maintenance

(A) Hematopoietic reconstitution capacity of BM cells (4×10^5) from donor mice of the indicated genotypes. Cells from donors harboring the Mx1-Cre transgene were harvested at 4 weeks after poly(I:C) injection. Data are means ± SD. ***$p < 0.005$.

We further performed long-term culture of KSL cells on a layer of OP9 stromal cells, with the number of colony-forming cells arising after 2 or 5 weeks of culture reflecting the function of hematopoietic progenitor or stem cells, respectively. The number of colonies derived from p57-deficient KSL cells was significantly decreased compared with that derived from control cells, although a similar assay with freshly isolated KSL cells without culture did not show a significant difference in the number of colonies formed (Figure 2F). The number of colonies derived from p21- or p27-deficient KSL cells did not differ significantly from that derived from the corresponding control cells with or without culture on OP9 cells. A serial replating assay revealed that the number of colonies derived from p57-deficient KSL cells declined to a greater extent compared with that of colonies derived from control cells with each plating, whereas the number of colonies derived from p21- or p27-deficient KSL cells did not differ significantly from that derived from the corresponding control cells at each plating (Figure S2). Collectively, these results suggested that the self-renewal capacity of HSCs was profoundly affected by the loss of p57, but not by that of p21 or p27.

p57 Is Required for Maintenance of Quiescence in HSCs

HSCs are normally maintained in an undifferentiated quiescent (G_0 phase) state, with this quiescence protecting the cells against loss of self-renewal capacity. To evaluate directly HSC quiescence in p57-deficient mice, we stained KSL cells from poly(I:C)-injected Mx1-Cre/$p57^{+/+}$ or Mx1-Cre/$p57^{+/F}$ mice with a combination of Hoechst 33342 and pyronin Y, which differentially and quantitatively stain DNA and RNA and thereby allow detection of cells in G_0 phase. We found that 28% of control KSL cells were negative for staining with pyronin Y, indicative of normal HSC quiescence, whereas only 15% of p57-deficient KSL cells were in G_0 phase (Figures 3A and 3B). No such difference was observed for p21- or p27-deficient KSL cells and the corresponding control cells. We also examined the cell cycle status of $CD34^-$KSL and $CD34^+$KSL cells on the basis of 5-bromodeoxyuridine (BrdU) incorporation. More $BrdU^+$ cells were detected among p57-deficient $CD34^-$KSL and $CD34^+$KSL populations than among the corresponding control cells (Figure 3C), consistent with the reduced size of the G_0 population for p57-deficient KSL cells. Furthermore, the frequency of apoptosis was substantially increased among p57-deficient KSL cells, but not among p21- or p27-deficient KSL cells (Figure 3D). Similar results were obtained 3 days after the onset of a shortened course of poly(I:C) treatment (Figures S3A–S3D). These results thus suggested that p57, but not p21 or p27, is essential for maintenance of HSC quiescence.

Immunofluoresence analysis revealed that the expression of p53 was increased in p57-deficient KSL cells (Figures S3E and S3F). Treatment of p57-deficient cells with the p53 inhibitor pifithrin-α resulted in suppression of apoptosis and significant restoration of their colony-forming ability (Figures S3G and S3H). Phosphorylation of the retinoblastoma protein (Rb) was increased in p57-deficient KSL cells compared with that in control cells, whereas no such difference was observed between the c-$Kit^+Sca\text{-}1^-Lin^-$ populations of the two genotypes (Figures 3E–3G). Treatment of p57-deficient KSL cells with the chemical CDK inhibitor SU9516, which is relatively specific for CDK2, reversed, at least in part, the changes in colony-forming ability, quiescence, and viability induced by loss of p57 (Figures 3H–3K), suggesting that increased CDK activity contributes to these effects of p57 deletion in KSL cells. Collectively, these results indicated that the loss of p57 results in exhaustion of HSCs, which is attributable in part to the induction of apoptosis mediated by upregulation of CDK activity and p53 expression.

Functional Overlap of p57 with Other CKIs

Although our data indicated that p57 is a key CKI in the determination of stemness of HSCs, it remained possible that other CKIs might partially compensate for the effects of p57 deficiency. To examine this possibility, we generated double-mutant mice that lack both p21 and p57 (Mx1-Cre/$p21^{-/-}$/$p57^{+/F}$ mice injected with poly(I:C)). Whereas deletion of p57 alone did not affect colony-forming activity of KSL cells in vitro before coculture with OP9 cells (Figure 2F), combined deletion of p21 and p57 resulted in a decrease in such colony formation (Figure 4A). Furthermore, the size of individual colonies was markedly smaller for the double mutant cells than for cells of poly(I:C)-injected Mx1-Cre/$p21^{+/+}$/$p57^{+/+}$ or Mx1-Cre/$p21^{+/+}$/$p57^{+/F}$ mice (Figure 4B). The number of colonies formed after coculture with OP9 cells was further decreased for the double-mutant KSL cells compared with that for p57-deficient KSL cells (Figure 4C). However, no significant difference in the percentage of cells in G_0 phase or in the frequency of apoptosis was apparent between KSL cells deficient in p57 alone and those deficient in both p21 and p57 (Figures 4D and 4E). Together, these results suggested that the combined deletion of both CKIs might affect not only HSCs but also progenitor cells. We also examined HSC function in mice lacking both p21 and p27. The number of colonies formed, the percentage of cells in quiescence, and the frequency of apoptosis did not differ significantly between KSL cells derived from $p21^{-/-}$/$p27^{-/-}$ mice and those derived from wild-type mice (Figures S4A–S4C).

Whereas the members of the Cip/Kip family of CKIs (p21, p27, p57) share a CKI domain that is essential for inhibition of CDKs,

(B and C) Hematopoietic reconstitution capacity of KSL cells (1.5×10^3) (B) or $CD150^+CD48^-$KSL cells (2×10^2) (C) derived from Mx1-Cre/$p57^{+/F}$ or control donor mice at 4 weeks after poly(I:C) injection. BM cells (2×10^6) from the recipient mice in (B) were serially transplanted into additional recipient mice. Data are means ± SD. ***$p < 0.005$.

(D) Frequency of donor-derived KSL cells among total BM cells of recipient mice in (B) at 16 weeks after transplantation. Data are means ± SD. ***$p < 0.005$.

(E) Irradiated recipient mice were transplanted with donor BM cells (4×10^5) from Mx1-Cre/$p57^{+/+}$ or Mx1-Cre/$p57^{+/F}$ mice (not injected with poly(I:C)) together with an equal number of competitor BM cells. The recipients were injected with poly(I:C) at 4 weeks after transplantation, and the percentage of donor-derived cells in peripheral blood was determined. Data are means ± SD. ***$p < 0.005$.

(F) In vitro colony formation capacity of KSL cells from mice of the indicated genotypes with or without prior coculture with OP9 cells. Cells from mice harboring the Mx1-Cre transgene were harvested at 4 weeks after poly(I:C) injection. Data are means ± SD. ***$p < 0.005$.

See also Figure S2.

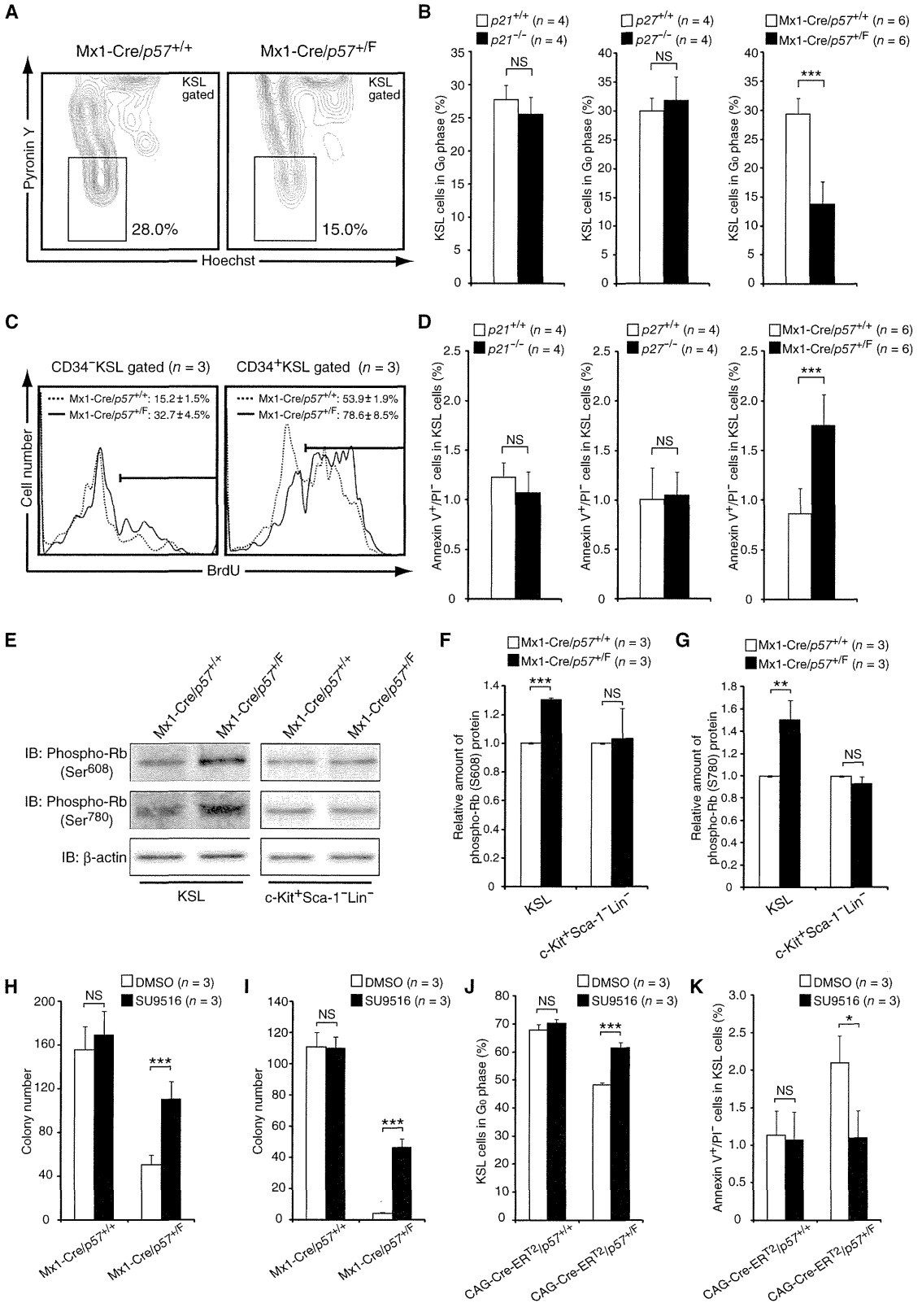

Figure 3. Loss of Quiescence and Induction of Apoptosis due to Increased CDK Activity in p57-Deficient HSCs

(A) Frequency of quiescence in KSL cells of Mx1-Cre/$p57^{+/+}$ and Mx1-Cre/$p57^{+/F}$ mice at 4 weeks after poly(I:C) injection. Quiescent cells were detected by staining with Hoechst 33342 and pyronin Y followed by flow cytometry.

p57 also contains a central domain that is absent in p21 and p27 and is thought to mediate functions other than inhibition of CDKs (Matsuoka et al., 1995). To test whether p57 function in the maintenance of HSCs is replaceable by p27, we examined the BM of $p57^{p27KI}$ mice, in which the p57 gene has been replaced with the p27 gene (Susaki et al., 2009). Similar to the pattern of p57 expression in wild-type mice, HA-tagged p27 encoded by the knockin allele at the p57 gene locus was expressed only in the KSL fraction, not in other more differentiated cells (Figure 4F). The size of the KSL population in $p57^{p27KI}$ mice was indistinguishable from that in wild-type mice (Figure 4G), and there was no difference in repopulating capacity at the first BMT, in colony formation in vitro with or without prior coculture with OP9 cells, or in the frequency of quiescence or apoptosis between HSCs of the two genotypes (Figures 4H–4K; Figure S4D). These results suggested that the total abundance of CKIs of the Cip/Kip family is an important determinant of HSC stemness.

DISCUSSION

We have examined the physiological importance of p57 in maintenance of HSCs by analysis of the effects of conditional deletion of p57 in mouse hematopoietic cells. Such mice lacking p57 manifested a reduction in the size of the HSC fraction as well as in the self-renewal capacity and G_0 population of KSL cells, effects that were not observed in mice lacking p21 or p27 (or both). We thus conclude that p57 plays the dominant role among Cip/Kip CKIs in the maintenance of HSCs.

The related CKIs p27 and p57 differ in the spatiotemporal patterns of their expression in many tissues and organs (Nagahama et al., 2001). Whereas p57 is most abundant in the HSC fraction of BM cells, its expression ceases as HSCs differentiate into progenitor cells. Expression of p27 is apparent in all hematopoietic fractions, whereas p21 is not detected in such cells in the absence of genotoxic stress. The expression patterns of these CKIs appear consistent with the phenotypes of the corresponding knockout mice. However, our present results suggest the existence of functional overlap between p57 and its related CKIs. The defects induced by p57 deficiency were thus reversed by p27 knockin, suggesting that the function of these CKIs at the molecular level is indistinguishable. We hypothesize that the specific response of cells to the lack of each CKI might be dependent on the total CKI abundance rather than on CKI type, but further investigation will be necessary to confirm this hypothesis. This relation between p27 and p57 in HSCs is similar to that observed in most (but not all) other tissues examined (Susaki et al., 2009).

Regulation of the cell cycle is thought to play a key role in the maintenance and function of HSCs. Mutant mice with deletions in genes for various cell cycle regulators thus manifest defects in HSC maintenance and function. The numbers of HSCs as well as common myeloid and lymphoid progenitors are decreased in mice with conditional inactivation of cyclin A2 (Kalaszczynska et al., 2009). The reconstitution ability of BM cells is also markedly impaired in these latter mutant mice. Likewise, mice lacking all D-type cyclins (cyclins D1, D2, and D3) show pronounced BM defects associated with a loss of the reconstitution capacity of BM cells; these animals develop severe anemia and die in utero (Kozar et al., 2004). Similar defects are apparent in mice deficient in both CDK4 and CDK6, which are the major partners of D-type cyclins (Malumbres et al., 2004). In contrast, no abnormality is apparent in mice lacking CDK2 (Berthet et al., 2007), suggesting that CDK1 may compensate for the loss of CDK2 (Aleem et al., 2005).

Rb is a major target of CDK2 and CDK4. Vav1-Cre/$Rb^{F/F}$ mice, which express Cre recombinase in hematopoietic cells, show a marked defect in the self-renewal competence and multipotency of HSCs (Daria et al., 2008), and deletion of all members of the Rb family (Rb, p107, and p130) further exacerbated this phenotype (Viatour et al., 2008). Mice deficient in E2F1, E2F2, and E2F3, all of which are downstream targets of Rb, show a decrease in the number of myeloid cells but maintain the function of HSCs (Viatour et al., 2008).

Some of the members of the Ink4 family of CKIs also contribute to the regulation of HSCs. Expression of $p16^{Ink4a}$ in HSCs increases with age, and the self-renewal capacity of HSCs does not decline with age in mice deficient in this CKI (Janzen et al., 2006). Mice lacking $p15^{Ink4b}$ do not exhibit an apparent defect in HSC function, although the proliferation of progenitors for granulocytes and monocytes is enhanced in these animals (Rosu-Myles et al., 2007). Loss of $p18^{Ink4c}$ results in expansion of the HSC pool associated with promotion of the cell cycle without loss of self-renewal capacity (Yuan et al., 2004). The effects of deletion of Ink4 CKIs thus appear opposite to those of deletion of Cip/Kip CKIs. Deletion of Cip/Kip CKIs results in

(B) Quantitative analysis of quiescent cells among KSL cells from mice of the indicated genotypes as determined from experiments similar to that in (A). Data are means ± SD. ***$p < 0.005$.

(C) Frequency of proliferating cells among $CD34^-$KSL and $CD34^+$KSL cells isolated from Mx1-Cre/$p57^{+/+}$ and Mx1-Cre/$p57^{+/F}$ mice at 4 weeks after poly(I:C) injection. Proliferating cells were detected by BrdU pulse-labeling analysis in vivo. The percentages of BrdU-positive cells are indicated as means ± SD.

(D) Quantitative analysis of apoptotic cells among KSL cells from mice of the indicated genotypes. Apoptotic cells in the KSL fraction were detected by staining with annexin V and propidium iodide (PI). Data are means ± SD. ***$p < 0.005$.

(E) Immunoblot analysis of phosphorylated Rb in KSL and c-Kit^+Sca-$1^-$$Lin^-$ cells from Mx1-Cre/$p57^{+/+}$ and Mx1-Cre/$p57^{+/F}$ mice at 4 weeks after poly(I:C) injection.

(F and G) Quantitative analysis of the relative amounts of Ser608-phosphorylated Rb (F) and Ser780-phosphorylated Rb (G) as determined from experiments similar to that in (E). Data are means ± SD. **$p < 0.01$, ***$p < 0.005$.

(H and I) Colony formation by KSL cells from Mx1-Cre/$p57^{+/+}$ and Mx1-Cre/$p57^{+/F}$ mice at 4 weeks after poly(I:C) injection after coculture on OP9 cells for 2 weeks (H) or 5 weeks (I) with 160 nM SU9516 or dimethyl sulfoxide (DMSO). Data are means ± SD. ***$p < 0.005$.

(J and K) Quantitative analysis of quiescent cells (J) and apoptotic cells (K) among KSL cells from CAG-Cre-ER^{T2}/$p57^{+/+}$ and CAG-Cre-ER^{T2}/$p57^{+/F}$ mice after culture for 2 weeks on OP9 cells, the second week in the presence of 1 μM 4-hydroxytamoxifen (4-OHT) and either 160 nM SU9516 or DMSO. Data are means ± SD. ***$p < 0.005$.

See also Figure S3.

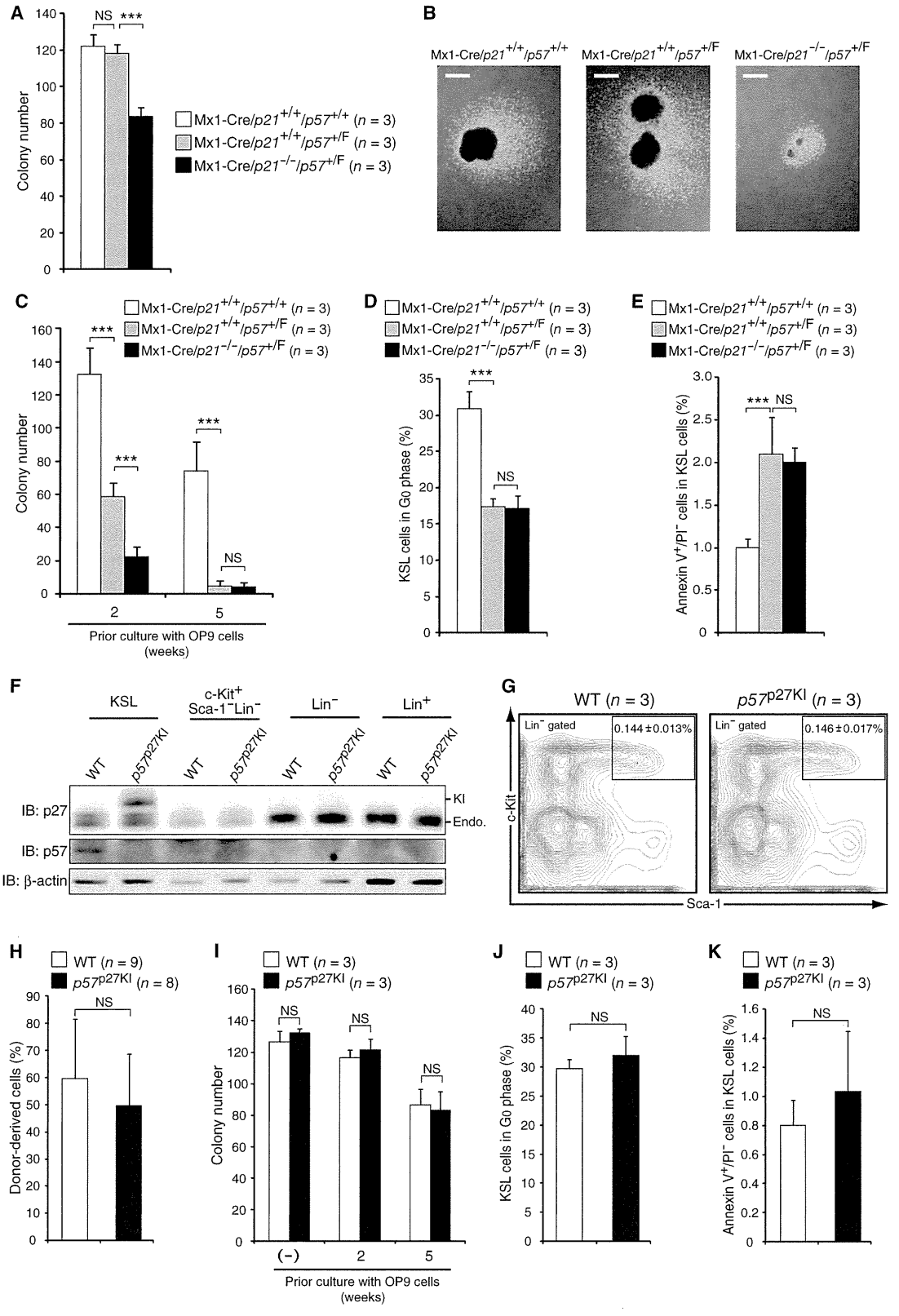

Figure 4. Overlap of CKI Function in HSC Maintenance

(A) In vitro colony formation capacity of KSL cells from mice of the indicated genotypes at 4 weeks after poly(I:C) injection. Data are means ± SD. ***p < 0.005.

(B) Representative colonies from the experiment shown in (A). Scale bars represent 0.5 mm.

exit of HSCs from the quiescent state and their entry into the proliferation cycle, an effect that is associated with the loss of self-renewal capacity or promotion of differentiation (or both).

The direct downstream targets of p27 and p57 CKIs are thought to be CDK2 and CDK4 (or CDK6), and inhibition of CDK activity by these CKIs maintains Rb in the unphosphorylated state (Halaban, 2005). Our results now show that the phosphorylation of Rb on Ser608 (phosphorylated by CDK2-cyclin A or E and CDK4-cyclin D) and Ser780 (phosphorylated by CDK4-cyclin D) (Halaban, 2005) was increased in p57-deficient KSL cells, suggesting that the activity of CDK2 or CDK4 (or both) is increased in KSL cells by deletion of p57.

We examined whether the effects of p57 deletion in HSCs are reversed by inhibition of CDK activity with the use of the chemical CDK inhibitor SU9516, which is relatively specific for CDK2 (Moshinsky et al., 2003). The in vitro colony formation capacity of KSL cells from poly(I:C)-injected Mx1-Cre/$p57^{+/F}$ mice was partially restored by treatment with SU9516 during prior coculture with OP9 cells, suggesting that increased activity of CDK2 is probably responsible for the effects of p57 deletion in KSL cells. The partial, rather than complete, restoration might be attributable to a contribution of CDK4 to the downregulation of colony formation ability in the p57-deficient KSL cells.

We have also shown that treatment of p57-deficient KSL cells with the p53 inhibitor pifithrin-α suppressed apoptosis and partially restored colony-forming ability. Furthermore, we have independently demonstrated that ablation of p57 results in hyperactivation of E2F1 and consequent p53-mediated apoptosis in mice (Susaki et al., 2009). Together, these lines of evidence support the notion that p57 deficiency results in abnormal upregulation of CDK activity, leading to hyperactivation of E2F1 and the triggering of p53-dependent apoptosis.

One of the substantial differences between fetal and adult HSCs is their dependency on quiescence: Maintenance of quiescence is thus thought to be more important for adult HSCs than for fetal HSCs. In an accompanying paper (Zou et al., 2011 [this issue of *Cell Stem Cell*]), HSCs in the fetal liver of conventional p27- or p57-deficient mice (Nakayama et al., 1996; Takahashi et al., 2000) were analyzed. Fetal HSCs lacking p57 did not manifest an apparent defect with the exception of a slight decrease in BM reconstitution capacity that was observed only after the third round of BM transfer. Combined deletion of p27 and p57 resulted in a marked failure in the maintenance of fetal HSCs, however, suggesting that these two CKIs have redundant roles. In contrast, our present study shows that p57 deficiency alone results in a substantial decrease in the number of adult HSCs as a result of their exit from quiescence and entry into apoptosis, with the BM reconstitution capacity of these p57-deficient cells also being greatly reduced from the first round of BM transfer. Deletion of p21 or p27 (or both proteins) did not result in any overt abnormalities in adult HSCs. Our analysis of mice lacking both p21 and p57 suggests that p21 also contributes to the maintenance of hematopoiesis, and that of $p57^{p27KI}$ mice suggests that p57 function in HSC maintenance can be replaced by p27. Collectively, our present study demonstrates that p57 plays a predominant role in constitutive maintenance of HSCs after birth.

EXPERIMENTAL PROCEDURES

Mice

Detailed methods for the generation of mice heterozygous for the floxed *p57* allele ($p57^{+/F}$ mice) as well as other mice used in this study are described in Supplemental Experimental Procedures. All mice were backcrossed with C57BL/6 mice more than six times. All mouse experiments were approved by the animal ethics committee of Kyushu University.

BM Reconstitution Assays

Unfractionated BM cells (4×10^5), sorted LSK cells (1.5×10^3), or sorted $CD150^+CD48^-LSK$ cells (2×10^2) from $p21^{-/-}$, $p27^{-/-}$, Mx1-Cre/$p57^{+/F}$, or corresponding littermate control mice (CD45.2) were transplanted into lethally irradiated C57BL/6 congenic (CD45.1) recipients together with competitor BM cells (4×10^5) from C57BL/6 heterozygous congenic (CD45.1/CD45.2) mice. For serial transplantation analysis, BM cells (2×10^6) were obtained from recipient mice at 16 weeks after transplantation (first BMT) and were transferred to a second set of lethally irradiated mice (second BMT).

Colony Formation Assays

Sorted KSL cells were subjected to colony formation assays with or without prior coculture with OP9 cells. Detailed methods for the assays are described in Supplemental Experimental Procedures.

SUPPLEMENTAL INFORMATION

Supplemental Information includes Supplemental Experimental Procedures and four figures and can be found with this article online at doi:10.1016/j.stem.2011.06.014.

ACKNOWLEDGMENTS

We thank P. Leder for p21-deficient mice, Y. Fukui for EIIa-Cre transgenic mice, D.R. Littman for pL2-Neo and pMC-Cre, T. Suda for sharing unpublished results, and Y. Matsuzaki, K. Shibata, A. Niihara, C. Mitai, Y. Yamada, K. Takeda, and M. Tanaka for technical assistance.

Received: December 13, 2010
Revised: June 1, 2011
Accepted: June 27, 2011
Published: September 1, 2011

(C) In vitro colony formation capacity of KSL cells from mice of the indicated genotypes after coculture with OP9 cells. Data are means ± SD. ***$p < 0.005$.
(D and E) Quantitative analysis of quiescent cells (D) and apoptotic cells (E) among KSL cells from mice of the indicated genotypes. Data are means ± SD. ***$p < 0.005$.
(F) Immunoblot analysis of fractionated hematopoietic cells from BM of wild-type (WT) and $p57^{p27KI}$ mice. The band positions for endogenous p27 (Endo.) and knocked-in hemagglutinin epitope-tagged p27 (KI) are shown.
(G) Frequency of KSL cells among BM cells of wild-type and $p57^{p27KI}$ mice. The percentages of KSL cells among total BM cells are shown as means ± SD.
(H) Hematopoietic reconstitution capacity of BM cells from $p57^{p27KI}$ and littermate control mice. Data are means ± SD.
(I) In vitro colony formation capacity of KSL cells from wild-type and $p57^{p27KI}$ mice with or without prior coculture with OP9 cells. Data are means ± SD.
(J and K) Quantitative analysis of quiescent cells (I) and apoptotic cells (J) among KSL cells from wild-type and $p57^{p27KI}$ mice. Data are means ± SD.
See also Figure S4.

REFERENCES

Aleem, E., Kiyokawa, H., and Kaldis, P. (2005). Cdc2-cyclin E complexes regulate the G1/S phase transition. Nat. Cell Biol. *7*, 831–836.

Arai, F., and Suda, T. (2007). Maintenance of quiescent hematopoietic stem cells in the osteoblastic niche. Ann. N Y Acad. Sci. *1106*, 41–53.

Berthet, C., Rodriguez-Galan, M.C., Hodge, D.L., Gooya, J., Pascal, V., Young, H.A., Keller, J., Bosselut, R., and Kaldis, P. (2007). Hematopoiesis and thymic apoptosis are not affected by the loss of Cdk2. Mol. Cell. Biol. *27*, 5079–5089.

Cheng, T., Rodrigues, N., Dombkowski, D., Stier, S., and Scadden, D.T. (2000a). Stem cell repopulation efficiency but not pool size is governed by $p27^{kip1}$. Nat. Med. *6*, 1235–1240.

Cheng, T., Rodrigues, N., Shen, H., Yang, Y., Dombkowski, D., Sykes, M., and Scadden, D.T. (2000b). Hematopoietic stem cell quiescence maintained by $p21^{cip1/waf1}$. Science *287*, 1804–1808.

Daria, D., Filippi, M.D., Knudsen, E.S., Faccio, R., Li, Z., Kalfa, T., and Geiger, H. (2008). The retinoblastoma tumor suppressor is a critical intrinsic regulator for hematopoietic stem and progenitor cells under stress. Blood *111*, 1894–1902.

Halaban, R. (2005). Rb/E2F: A two-edged sword in the melanocytic system. Cancer Metastasis Rev. *24*, 339–356.

Janzen, V., Forkert, R., Fleming, H.E., Saito, Y., Waring, M.T., Dombkowski, D.M., Cheng, T., DePinho, R.A., Sharpless, N.E., and Scadden, D.T. (2006). Stem-cell ageing modified by the cyclin-dependent kinase inhibitor $p16^{INK4a}$. Nature *443*, 421–426.

Kalaszczynska, I., Geng, Y., Iino, T., Mizuno, S., Choi, Y., Kondratiuk, I., Silver, D.P., Wolgemuth, D.J., Akashi, K., and Sicinski, P. (2009). Cyclin A is redundant in fibroblasts but essential in hematopoietic and embryonic stem cells. Cell *138*, 352–365.

Kozar, K., Ciemerych, M.A., Rebel, V.I., Shigematsu, H., Zagozdzon, A., Sicinska, E., Geng, Y., Yu, Q., Bhattacharya, S., Bronson, R.T., et al. (2004). Mouse development and cell proliferation in the absence of D-cyclins. Cell *118*, 477–491.

Lakso, M., Pichel, J.G., Gorman, J.R., Sauer, B., Okamoto, Y., Lee, E., Alt, F.W., and Westphal, H. (1996). Efficient in vivo manipulation of mouse genomic sequences at the zygote stage. Proc. Natl. Acad. Sci. USA *93*, 5860–5865.

Malumbres, M., Sotillo, R., Santamaría, D., Galán, J., Cerezo, A., Ortega, S., Dubus, P., and Barbacid, M. (2004). Mammalian cells cycle without the D-type cyclin-dependent kinases Cdk4 and Cdk6. Cell *118*, 493–504.

Matsuoka, S., Edwards, M.C., Bai, C., Parker, S., Zhang, P., Baldini, A., Harper, J.W., and Elledge, S.J. (1995). $p57^{KIP2}$, a structurally distinct member of the $p21^{CIP1}$ Cdk inhibitor family, is a candidate tumor suppressor gene. Genes Dev. *9*, 650–662.

Miyamoto, K., Araki, K.Y., Naka, K., Arai, F., Takubo, K., Yamazaki, S., Matsuoka, S., Miyamoto, T., Ito, K., Ohmura, M., et al. (2007). Foxo3a is essential for maintenance of the hematopoietic stem cell pool. Cell Stem Cell *1*, 101–112.

Moshinsky, D.J., Bellamacina, C.R., Boisvert, D.C., Huang, P., Hui, T., Jancarik, J., Kim, S.H., and Rice, A.G. (2003). SU9516: Biochemical analysis of cdk inhibition and crystal structure in complex with cdk2. Biochem. Biophys. Res. Commun. *310*, 1026–1031.

Nagahama, H., Hatakeyama, S., Nakayama, K., Nagata, M., Tomita, K., and Nakayama, K. (2001). Spatial and temporal expression patterns of the cyclin-dependent kinase (CDK) inhibitors $p27^{Kip1}$ and $p57^{Kip2}$ during mouse development. Anat. Embryol. (Berl.) *203*, 77–87.

Nakayama, K., Ishida, N., Shirane, M., Inomata, A., Inoue, T., Shishido, N., Horii, I., Loh, D.Y., and Nakayama, K.I. (1996). Mice lacking $p27^{Kip1}$ display increased body size, multiple organ hyperplasia, retinal dysplasia, and pituitary tumors. Cell *85*, 707–720.

Pawliuk, R., Eaves, C., and Humphries, R.K. (1996). Evidence of both ontogeny and transplant dose-regulated expansion of hematopoietic stem cells in vivo. Blood *88*, 2852–2858.

Qian, H., Buza-Vidas, N., Hyland, C.D., Jensen, C.T., Antonchuk, J., Månsson, R., Thoren, L.A., Ekblom, M., Alexander, W.S., and Jacobsen, S.E.W. (2007). Critical role of thrombopoietin in maintaining adult quiescent hematopoietic stem cells. Cell Stem Cell *1*, 671–684.

Rosu-Myles, M., Taylor, B.J., and Wolff, L. (2007). Loss of the tumor suppressor $p15^{Ink4b}$ enhances myeloid progenitor formation from common myeloid progenitors. Exp. Hematol. *35*, 394–406.

Sherr, C.J., and Roberts, J.M. (2004). Living with or without cyclins and cyclin-dependent kinases. Genes Dev. *18*, 2699–2711.

Susaki, E., Nakayama, K., Yamasaki, L., and Nakayama, K.I. (2009). Common and specific roles of the related CDK inhibitors p27 and p57 revealed by a knock-in mouse model. Proc. Natl. Acad. Sci. USA *106*, 5192–5197.

Takahashi, K., Nakayama, K., and Nakayama, K.I. (2000). Mice lacking a CDK inhibitor, $p57^{Kip2}$, exhibit skeletal abnormalities and growth retardation. J. Biochem. *127*, 73–83.

van Os, R., Kamminga, L.M., Ausema, A., Bystrykh, L.V., Draijer, D.P., van Pelt, K., Dontje, B., and de Haan, G. (2007). A limited role for $p21^{Cip1/Waf1}$ in maintaining normal hematopoietic stem cell functioning. Stem Cells *25*, 836–843.

Viatour, P., Somervaille, T.C., Venkatasubrahmanyam, S., Kogan, S., McLaughlin, M.E., Weissman, I.L., Butte, A.J., Passegué, E., and Sage, J. (2008). Hematopoietic stem cell quiescence is maintained by compound contributions of the retinoblastoma gene family. Cell Stem Cell *3*, 416–428.

Yamazaki, S., Iwama, A., Takayanagi, S.I., Morita, Y., Eto, K., Ema, H., and Nakauchi, H. (2006). Cytokine signals modulated via lipid rafts mimic niche signals and induce hibernation in hematopoietic stem cells. EMBO J. *25*, 3515–3523.

Yan, Y., Frisén, J., Lee, M.H., Massagué, J., and Barbacid, M. (1997). Ablation of the CDK inhibitor $p57^{Kip2}$ results in increased apoptosis and delayed differentiation during mouse development. Genes Dev. *11*, 973–983.

Yuan, Y.Z., Shen, H.M., Franklin, D.S., Scadden, D.T., and Cheng, T. (2004). In vivo self-renewing divisions of haematopoietic stem cells are increased in the absence of the early G1-phase inhibitor, $p18^{INK4C}$. Nat. Cell Biol. *6*, 436–442.

Zhang, P., Liégeois, N.J., Wong, C., Finegold, M., Hou, H., Thompson, J.C., Silverman, A., Harper, J.W., DePinho, R.A., and Elledge, S.J. (1997). Altered cell differentiation and proliferation in mice lacking $p57^{KIP2}$ indicates a role in Beckwith-Wiedemann syndrome. Nature *387*, 151–158.

Zou, P., Arai, F., Yoshihara, H., Tai, I., Hosokawa, K., Matsumoto, Y., Shinmyozu, K., Tsukahara, F., Maru, Y., Nakayama, K., et al. (2011). $p57^{Kip2}$ and $p57^{Kip1}$ cooperate to maintain hematopoietic stem cell quiescence through interactions with Hsc70. Cell Stem Cell *9*, this issue, 247–261.

Cell Metabolism
Article

The FBXL5-IRP2 Axis Is Integral to Control of Iron Metabolism In Vivo

Toshiro Moroishi,[1,2] Masaaki Nishiyama,[1,2] Yukiko Takeda,[2,3] Kazuhiro Iwai,[2,3] and Keiichi I. Nakayama[1,2,*]
[1]Department of Molecular and Cellular Biology, Medical Institute of Bioregulation, Kyushu University, 3-1-1 Maidashi, Higashi-ku, Fukuoka, Fukuoka 812-8582, Japan
[2]CREST, Japan Science and Technology Agency (JST), Kawaguchi, Saitama 332-0012, Japan
[3]Department of Biophysics and Biochemistry, Graduate School of Medicine, and Cell Biology and Metabolism Group, Graduate School of Frontier Biosciences, Osaka University, Suita, Osaka 565-0871, Japan
*Correspondence: nakayak1@bioreg.kyushu-u.ac.jp
DOI 10.1016/j.cmet.2011.07.011

SUMMARY

Iron-dependent degradation of iron-regulatory protein 2 (IRP2) is a key event for maintenance of an appropriate intracellular concentration of iron. Although FBXL5 (F box and leucine-rich repeat protein 5) is thought to mediate this degradation, the role of FBXL5 in the control of iron homeostasis in vivo has been poorly understood. We have now found that mice deficient in FBXL5 died in utero, associated with excessive iron accumulation. This embryonic mortality was prevented by additional ablation of IRP2, suggesting that impaired IRP2 degradation is primarily responsible for the death of *Fbxl5*$^{-/-}$ mice. We also found that liver-specific deletion of *Fbxl5* resulted in deregulation of both hepatic and systemic iron homeostasis, leading to the development of steatohepatitis. The liver-specific mutant mice died with acute liver failure when fed a high-iron diet. Thus, our results uncover a major role for FBXL5 in ensuring an appropriate supply of iron to cells.

INTRODUCTION

Iron is an essential cofactor for many proteins that function in oxygen transport, cellular respiration, or DNA synthesis (Rouault and Tong, 2005), with iron deficiency resulting in cellular growth arrest and death. Conversely, the chemical properties of iron give rise to side reactions that damage macromolecules (Hentze et al., 2010). Thus, excess ferrous iron reacts with hydrogen peroxide or lipid peroxides to generate hydroxyl and lipid radicals, respectively. These oxygen metabolites react readily with biological molecules including proteins, lipids, and DNA. Given that both iron deficiency and iron overload are deleterious to cells, defects in iron acquisition at the cellular and systemic levels lead to human disorders (De Domenico et al., 2008). Thus, iron homeostasis is strictly controlled to ensure provision of a proper amount of iron to cells.

The control of systemic iron homeostasis occurs through regulation of iron acquisition (Andrews and Schmidt, 2007), given that iron loss occurs only through exfoliation and blood loss. Plasma iron levels are determined predominantly by the amount of duodenal iron absorption and by iron release from macrophages that recycle iron from senescent red blood cells (Wang and Pantopoulos, 2011). These iron fluxes are precisely regulated by hepcidin, a small peptide hormone released from the liver that is also known as Hamp1 or Leap1. Hepcidin negatively regulates iron transport into plasma by controlling the expression of an iron exporter, ferroportin (Nemeth et al., 2004). Thus, systemic iron metabolism is maintained in balance by the hepcidin-ferroportin regulatory system.

At the cellular level, iron homeostasis is regulated by coordination of iron uptake, storage, export, and utilization (Hentze et al., 2010). Iron is imported into cells in the ferrous form and accumulates as a cytosolic labile iron pool (LIP) that is essential for direct incorporation of iron into proteins or for its transport into mitochondria, which constitute a major site of iron utilization. Ferrous iron from the LIP that is not utilized for metalation reactions is exported by ferroportin or stored in a redox-inactive form (ferric iron) bound to ferritin, thereby preventing iron-mediated cell damage. Thus, the size of the LIP is determined by the rates of iron uptake, storage, export, and utilization, and these processes must be strictly regulated to prevent deleterious iron deficiency or excess.

The abundance of some proteins that contribute to determination of the size of the LIP is regulated at the posttranscriptional level by iron-regulatory protein 1 (IRP1) and IRP2 (Muckenthaler et al., 2008). These RNA-binding proteins interact with conserved *cis*-regulatory hairpin structures known as iron-responsive elements (IREs) during iron-limiting conditions to regulate the translation and stability of mRNAs that encode proteins required for iron homeostasis. IRP1 (but not IRP2) is a bifunctional protein: in the apo-IRP1 form, it binds to IREs and thereby controls gene expression; however, it also assembles to form a [4Fe-4S] cluster that does not bind IREs and thereby becomes cytosolic aconitase (holo-IRP1) under iron-sulfur cluster-replete conditions. Both apo-IRP1 and IRP2 inhibit initiation of translation when they are bound to IREs in the 5′ untranslated regions of mRNAs for the H or L chains of ferritin (which mediate iron storage), for ferroportin (which mediates iron export), or for aminolevulinic acid synthase 2 (Alas2, which mediates iron utilization), whereas their binding to the IRE in the 3′ untranslated region of the mRNA for transferrin receptor 1 (TfR1, which mediates iron uptake) prevents its degradation.

As a consequence of these interactions, IRPs increase the size of the LIP (ferrous iron) during iron-limiting conditions. In contrast, under iron-replete conditions, IRPs are degraded by the proteasome, leading to a decrease in the size of the cytosolic LIP. Thus, iron-dependent degradation of IRPs in iron-replete cells is a key event in the maintenance of an appropriate intracellular concentration of iron.

An iron- and oxygen-regulated SCF-type ubiquitin ligase (E3), SCF^{FBXL5}, has been shown to contribute to iron-dependent degradation of IRP1 and IRP2 (Salahudeen et al., 2009; Vashisht et al., 2009). FBXL5 (F box and leucine-rich repeat protein 5) is a member of the F box family of proteins that confer substrate specificity on SCF-type ubiquitin ligases (Jin et al., 2004; Nakayama and Nakayama, 2006). FBXL5 contains a unique hemerythrin domain that is related to a family of iron- and oxygen-binding proteins in bacteria and invertebrates. Direct binding of iron to the hemerythrin domain stabilizes FBXL5, which is unstable under iron-deficient conditions. Thus, such binding results in the degradation of IRPs by the stabilized FBXL5 under iron-replete conditions. However, despite its integral role in IRP degradation, the biological relevance of FBXL5 as well as its effects on iron homeostasis have remained unknown.

We have now inactivated the mouse FBXL5 gene globally and selectively. Our characterization of these FBXL5-deficient mice has revealed that FBXL5 plays a pivotal role in the maintenance of appropriate concentrations of intracellular iron and that it is essential both for embryonic development and for normal postnatal liver physiology. Loss of FBXL5 in mice induced apoptosis as a result of unrestrained IRP activity, and consistent with this finding, deletion of *Irp2* in *Fbxl5*$^{-/-}$ mice prevented their embryonic death. Our results indicate that the FBXL5-IRP2 axis is integral to iron homeostasis in vivo.

RESULTS

Loss of FBXL5 Results in Embryonic Mortality in Mice

To elucidate the physiological functions of FBXL5, we generated mice deficient in this protein. The FBXL5 gene was disrupted in mouse embryonic stem cells (ESCs) by replacement of exons 4 and 5, which encode the F box domain, with IRES-*lacZ* and PGK-*neo*-poly(A)-loxP cassettes (see Figure S1 available online). Mice heterozygous for the *Fbxl5* mutant allele were healthy, fertile, and phenotypically indistinguishable from wild-type littermates. In contrast no homozygous mutants were detected among 372 newborn animals generated from heterozygote crosses, even though the ratio of wild-type to heterozygous offspring was normal (Figure 1A). Thus, the mutation appeared to be embryonic lethal in the homozygous state. Whole-mount in situ hybridization analysis revealed that FBXL5 mRNA was present throughout wild-type embryos from embryonic day (E) 7.5 to E8.5 but that it was localized predominantly in the brain from E9.5 to E11.5 (Figure 1B). No hybridization signal was detected in *Fbxl5*$^{-/-}$ embryos (Figure 1C).

To determine the time at which the *Fbxl5* mutation becomes lethal, we examined embryos from *Fbxl5*$^{+/-}$ intercrosses at various developmental stages (Figure 1A). Most *Fbxl5*$^{-/-}$ embryos underwent resorption manifesting growth retardation and massive hemorrhage at E8.5 and thereafter, although the mutant embryos appeared normal at E7.5 (Figure 1D). Histopathologic examination revealed that *Fbxl5*$^{+/-}$ and *Fbxl5*$^{-/-}$ embryos were indistinguishable at E7.5, with each egg cylinder consisting of three layers of tissue (ectoderm, mesoderm, and visceral endoderm) (Figure 1E). However, *Fbxl5*$^{-/-}$ embryos manifested growth retardation and were inviable at E8.5. Apoptotic cells with condensed nuclei as well as hemorrhage in the region of the ectoplacental cone were typically observed in the *Fbxl5*$^{-/-}$ embryos. Thus, these results suggested that FBXL5 is essential for early embryonic development.

Fatal Iron Accumulation in *Fbxl5*$^{-/-}$ Embryos

To explore the cause of the abnormal cell death observed in the ectoplacental cone of *Fbxl5*$^{-/-}$ embryos, we performed diaminobenzidine (DAB)-enhanced Perls staining and DAB-enhanced Turnbull staining, which are specific for ferric and ferrous iron, respectively (Meguro et al., 2003) (Figure 2A). Both Perls- and Turnbull-positive iron deposits were observed in the ectoplacental cone of *Fbxl5*$^{-/-}$ embryos at E8.5, suggesting that ferrous iron accumulated in these embryos. Furthermore, ferrous iron deposits were also observed in the extraembryonic visceral endoderm of *Fbxl5*$^{-/-}$ embryos at E7.5, before morphological changes were apparent.

The extraembryonic visceral endoderm and the ectoplacental cone function as an early placenta in maternoembryonic nutrient transport before formation of the placenta proper (Cross et al., 1994). Given that iron is supplied to the embryo through this early placenta, we hypothesized that the loss of FBXL5 might result in iron overload in the early placenta, leading to oxidative stress. A marked increase in the abundance of cytoplasmic 4-hydroxy-2-nonenal (4-HNE)-modified proteins, an indicator of oxidative stress, was apparent as early as E7.5 in the extraembryonic visceral endoderm of *Fbxl5*$^{-/-}$ embryos, compared with that in *Fbxl5*$^{+/-}$ embryos (Figure 2B). Although the TUNEL (terminal deoxynucleotidyl transferase-mediated dUTP nick-end labeling) assay did not detect apoptotic cells at E7.5 (Figure S2A), several apoptotic cells were apparent in the ectoplacental cone as well as in the embryonic portion of *Fbxl5*$^{-/-}$ embryos at E8.5 (Figure 2C). These results suggested that the loss of FBXL5 results in iron overload, leading to oxidative stress and apoptosis, in the early embryo.

To assess directly the growth capability of *Fbxl5*$^{-/-}$ embryos independent of placental function, we examined the outgrowth of blastocysts in culture. All *Fbxl5*$^{+/+}$, *Fbxl5*$^{+/-}$, and *Fbxl5*$^{-/-}$ blastocysts hatched, attached to the culture dish, and produced apparently normal trophoblast giant cells and an inner cell mass under normal iron conditions (Figure S2B), suggesting that *Fbxl5*$^{-/-}$ blastocysts develop normally in the absence of iron stress. However, under high-iron conditions, development of both the trophectoderm and inner cell mass by *Fbxl5*$^{-/-}$ blastocysts was impaired, with this impairment being prevented by the presence of the antioxidant *N*-acetyl-L-cysteine (NAC) (Figure 2D). Thus, these observations indicated that not only the early placenta but also embryonic tissue is damaged by iron overload and consequent oxidative stress in the absence of FBXL5.

IRP Accumulation in FBXL5-Deficient Mice

Given that iron accumulation was observed in *Fbxl5*$^{-/-}$ embryos, we hypothesized that upregulation of IRPs might be

A

Embryonic day	No. of animals recoverable			Total no. of animals
	Fbxl5$^{+/+}$	*Fbxl5*$^{+/-}$	*Fbxl5*$^{-/-}$ (no. resorbed)	
E3.5	3	12	6 (0)	21
E7.5	18	29	9 (0)	56
E8.5	11	19	4 (4)	34
E9.5	4	17	7 (7)	28
E11.5	8	14	8 (8)	30
E13.5	15	33	12 (12)	60
Newborn	132	240	0 (0)	372

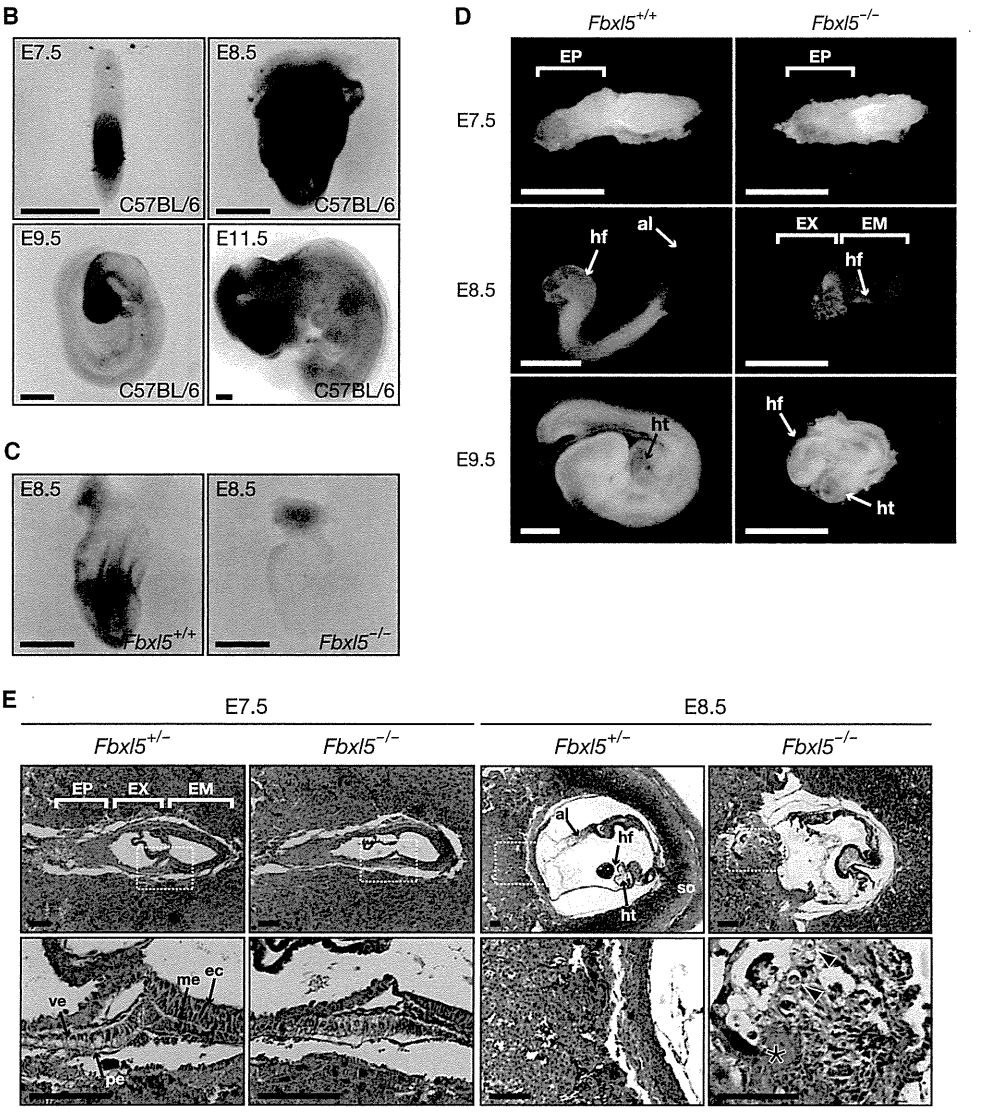

Figure 1. Targeted Disruption of *Fbxl5* Results in Embryonic Death

(A) Genotype frequencies for total embryos and live offspring produced from *Fbxl5*$^{+/-}$ mouse intercrosses. Numbers in parentheses indicate resorbed embryos.

(B) Whole-mount in situ hybridization of C57BL/6 embryos at E7.5, E8.5, E9.5, and E11.5 with a riboprobe specific for FBXL5 mRNA. Scale bars, 500 μm.

(C) Whole-mount in situ hybridization of *Fbxl5*$^{+/+}$ and *Fbxl5*$^{-/-}$ embryos at E8.5 with an FBXL5 riboprobe. Scale bars, 500 μm.

(D) Gross appearance of *Fbxl5*$^{+/+}$ versus *Fbxl5*$^{-/-}$ embryos at E7.5, E8.5, and E9.5. EP, ectoplacental cone; EX, extraembryonic portion; EM, embryonic portion; hf, headfold; al, allantois; ht, heart. Scale bars, 500 μm.

(E) Histopathology of *Fbxl5*$^{-/-}$ embryos. The development of *Fbxl5*$^{+/-}$ and *Fbxl5*$^{-/-}$ embryos is shown at E7.5 and E8.5. The boxed regions in the upper panels are shown at higher magnification in the lower panels. Apoptotic cells with condensed nuclei (arrowheads) as well as hemorrhage and fibrin (asterisk) in the area of the ectoplacental cone are indicated. ec, ectoderm; me, mesoderm; pe, parietal endoderm; ve, visceral endoderm; so, somites. Scale bars, 100 μm. See also Figure S1.

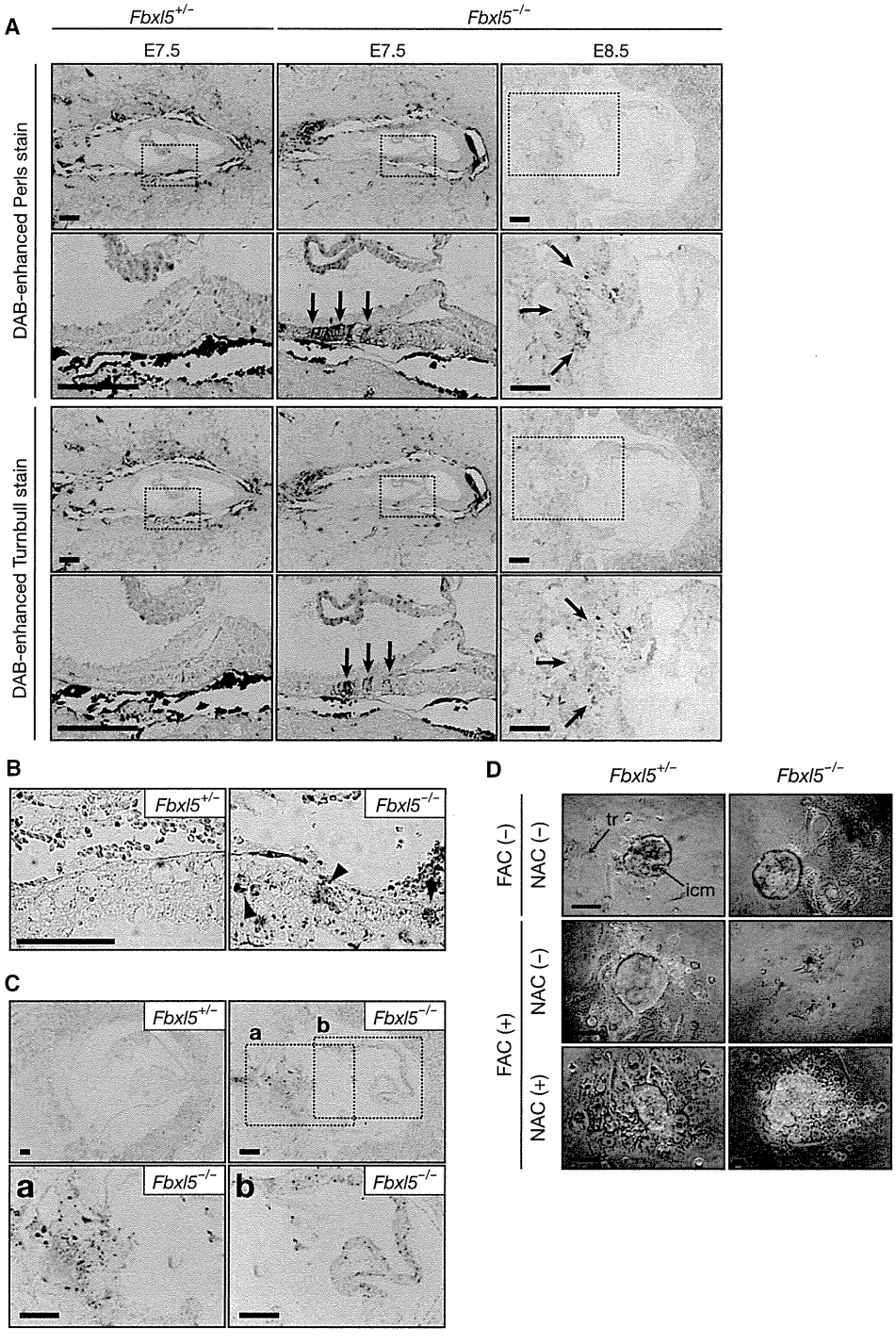

Figure 2. Fatal Iron Accumulation and Oxidative Stress in *Fbxl5*$^{-/-}$ Embryos

(A) DAB-enhanced Perls staining (top panels) and DAB-enhanced Turnbull staining (bottom panels) of *Fbxl5*$^{+/-}$ (E7.5) and *Fbxl5*$^{-/-}$ (E7.5 and E8.5) embryos. The boxed regions in the upper panels of each set are shown at higher magnification in the lower panels. Brown staining indicates iron accumulation in the extra-embryonic visceral endoderm (E7.5) or ectoplacental cone (E8.5) of *Fbxl5*$^{-/-}$ embryos (arrows). Scale bars, 100 μm.

(B) Sections of *Fbxl5*$^{+/-}$ and *Fbxl5*$^{-/-}$ embryos at E7.5 were subjected to immunohistochemical staining with antibodies to 4-HNE. Arrowheads indicate an increased staining intensity for 4-HNE-modified proteins in the extraembryonic visceral endoderm of the *Fbxl5*$^{-/-}$ embryo. Scale bar, 50 μm.

(C) Sections of *Fbxl5*$^{+/-}$ and *Fbxl5*$^{-/-}$ embryos at E8.5 were subjected to the TUNEL assay. Higher-magnification views of the ectoplacental cone (a) and embryonic portion (b) of the *Fbxl5*$^{-/-}$ embryo are also shown. Scale bars, 100 μm.

(D) Blastocysts from *Fbxl5*$^{+/-}$ mouse intercrosses were cultured in the absence or presence of ferric ammonium citrate (FAC, 50 μg/ml) or NAC (1 mM) for 5 days in vitro. The development of *Fbxl5*$^{+/-}$ and *Fbxl5*$^{-/-}$ blastocysts was examined at E8.5. icm, inner cell mass; tr, trophectoderm. Scale bars, 100 μm. See also Figure S2.

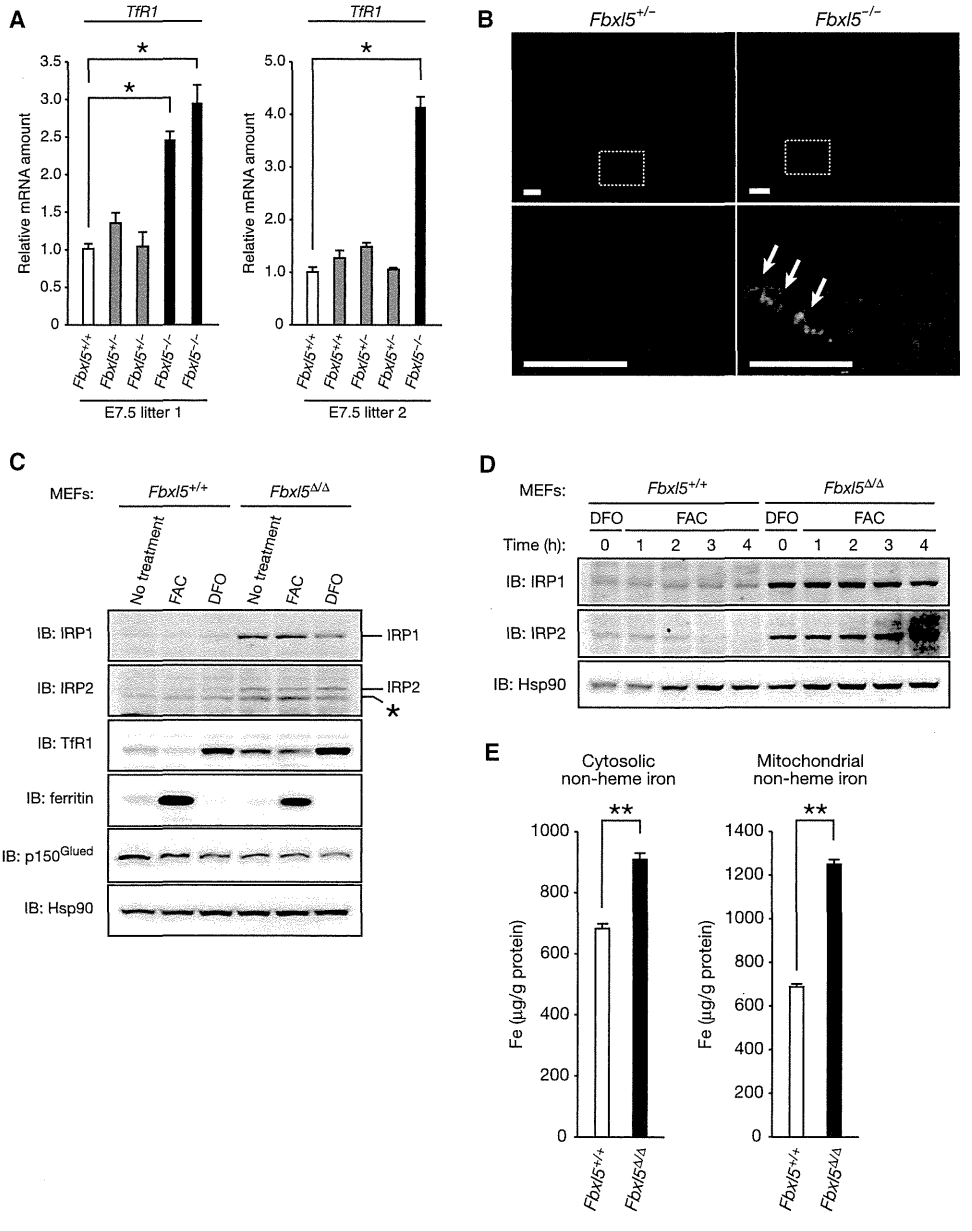

Figure 3. Accumulation of IRPs in FBXL5-Deficient Mice

(A) RT and real-time PCR analysis of TfR1 mRNA in littermate embryos of *Fbxl5*$^{+/-}$ mouse intercrosses at E7.5. Normalized data are expressed relative to the corresponding value for a control *Fbxl5*$^{+/+}$ embryo and are mean ± SEM from three independent experiments. *$p < 0.03$ (Student's t test).

(B) Sections of *Fbxl5*$^{+/-}$ and *Fbxl5*$^{-/-}$ embryos at E7.5 were subjected to immunohistofluorescence analysis with antibodies to TfR1. The boxed regions in the upper panels are shown at higher magnification in the lower panels. Arrows indicate an increased staining intensity for TfR1 in the extraembryonic mesoderm of the *Fbxl5*$^{-/-}$ embryo. Scale bars, 50 μm.

(C) *Fbxl5*$^{+/+}$ or *Fbxl5*$^{\Delta/\Delta}$ MEFs were incubated for 16 hr in the absence or presence of FAC (100 μg/ml) or 100 μM of the ferric-iron chelator desferrioxamine (DFO) and were then subjected to immunoblot (IB) analysis with antibodies to the indicated proteins. The asterisk indicates a nonspecific band.

(D) Immunoblot analysis of IRP1 and IRP2 in cells exposed to iron. *Fbxl5*$^{+/+}$ or *Fbxl5*$^{\Delta/\Delta}$ MEFs were incubated for 16 hr with 100 μM DFO and then exposed to FAC (50 μg/ml) for the indicated times.

(E) Total nonheme iron levels in cytosolic and mitochondrial fractions prepared from *Fbxl5*$^{+/+}$ or *Fbxl5*$^{\Delta/\Delta}$ MEFs that had been exposed to FAC (100 μg/ml) for 48 hr. Data are mean ± SD from three independent experiments. **$p < 0.01$ (Student's t test). See also Figure S3.

responsible for this deregulation of iron homeostasis. Therefore, we examined the abundance of TfR1 mRNA, a downstream target of IRPs, in the mutant embryos. The amount of TfR1 mRNA was markedly increased in *Fbxl5*$^{-/-}$ embryos (Figure 3A). Immunostaining also revealed that TfR1 accumulated in the extraembryonic mesoderm of *Fbxl5*$^{-/-}$ embryos at E7.5 (Figure 3B). Thus, these results suggested that IRP activity is increased, resulting in deregulation of IRP target genes, in *Fbxl5*$^{-/-}$ embryos.

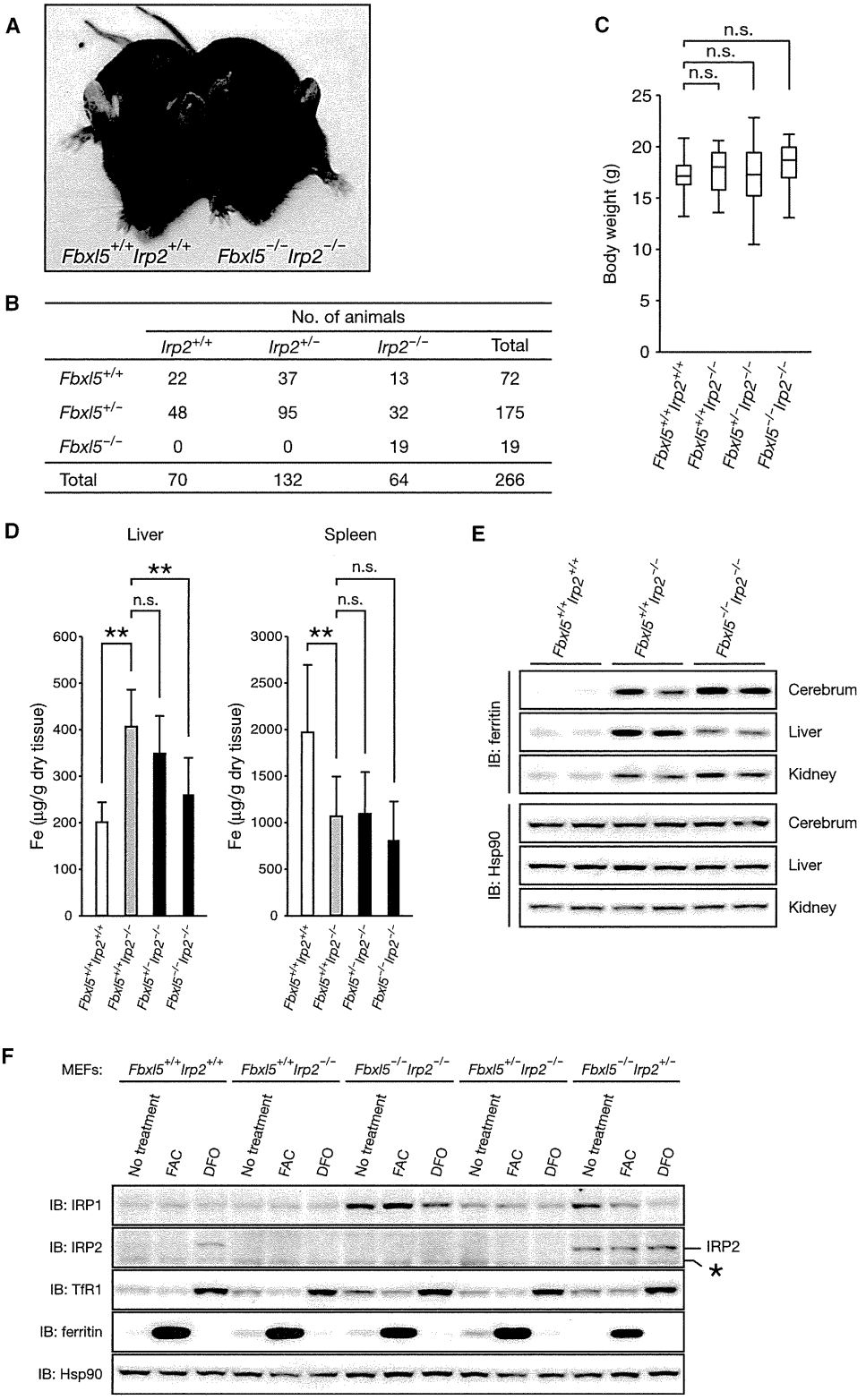

Figure 4. Prevention of Embryonic Mortality in FBXL5-Deficient Mice by Ablation of IRP2

(A) Gross appearance of *Fbxl5*$^{+/+}$*Irp2*$^{+/+}$ versus *Fbxl5*$^{-/-}$*Irp2*$^{-/-}$ littermates at 5 weeks of age.

(B) Genotype frequencies of 4-week-old mice produced from *Fbxl5*$^{+/-}$*Irp2*$^{+/-}$ mouse intercrosses.

(C) Box plot with whiskers from minimum to maximum body weight in *Fbxl5*$^{+/+}$*Irp2*$^{+/+}$ (n = 22), *Fbxl5*$^{+/+}$*Irp2*$^{-/-}$ (n = 10), *Fbxl5*$^{+/-}$*Irp2*$^{-/-}$ (n = 26), and *Fbxl5*$^{-/-}$*Irp2*$^{-/-}$ (n = 15) mice at 4 weeks of age. n.s., not significant ($p > 0.05$, Student's t test).

The early embryonic mortality of the *Fbxl5*$^{-/-}$ mutant impeded in-depth analysis of the role of FBXL5 in iron homeostasis. To overcome this obstacle, we generated mice in which *Fbxl5* is conditionally ablated in a tissue-specific manner. To this end, we first produced mice harboring a "floxed" allele of *Fbxl5*, in which exons 4 and 5 are flanked by loxP sites (Figures S3A–S3C). Mice homozygous for the floxed *Fbxl5* allele (*Fbxl5*$^{F/F}$ mice) had no apparent defects, indicating that the allele is fully functional.

To investigate whether iron-dependent degradation of IRPs is impaired in FBXL5-deficient mice, we prepared mouse embryonic fibroblasts (MEFs) from *Fbxl5*$^{+/+}$ and *Fbxl5*$^{F/F}$ embryos at E13.5 and subsequently infected these cells with a retroviral vector encoding Cre recombinase. We confirmed that almost all floxed alleles were deleted by Cre recombinase in the MEFs from *Fbxl5*$^{F/F}$ embryos, giving rise to *Fbxl5*$^{\Delta/\Delta}$ MEFs (Figure S3D). Immunoblot analysis revealed that the abundance of IRP1 and IRP2 was increased in *Fbxl5*$^{\Delta/\Delta}$ MEFs, whereas that of the other potential substrate of FBXL5, p150^{Glued} (Zhang et al., 2007), was not (Figure 3C). Such IRP accumulation was apparent even under iron-replete conditions. Consistent with this finding, the expression of proteins encoded by mRNA targets of IRPs was also deregulated: thus, the abundance of TfR1 (which mediates iron uptake) was increased, whereas that of ferritin (which mediates iron storage) was decreased likely as a result of IRP-mediated translational suppression (Figure 3C). However, the transcription of ferritin genes is also regulated by oxidative stress through an antioxidant-responsive element (ARE) in the 5′ region (MacKenzie et al., 2008). Indeed, the expression of ferritin was markedly increased at both mRNA (Figure S3E) and protein (Figure 3C) levels in *Fbxl5*$^{\Delta/\Delta}$ MEFs under the iron-replete condition, suggesting that transcriptional activation of ferritin genes by oxidative stress dominates the translational suppression mediated by constitutively active IRPs. Furthermore, the iron-dependent degradation of IRP2 was impaired in *Fbxl5*$^{\Delta/\Delta}$ MEFs (Figure 3D). Although the abundance of IRP1 in *Fbxl5*$^{\Delta/\Delta}$ MEFs was markedly increased compared with that in *Fbxl5*$^{+/+}$ MEFs, the half-life of this protein was long even in iron-replete *Fbxl5*$^{+/+}$ MEFs (Figure 3D), probably reflecting the fact that most IRP1s exist in the holo-IRP1 form, which is resistant to degradation in iron-replete cells (Recalcati et al., 2006). These results suggested that IRPs accumulate, resulting in an increase in total IRP activity, in FBXL5-deficient embryos and MEFs in a manner independent of iron conditions, leading to deregulation of IRP targets.

We next examined how such IRP hyperactivation affects cellular iron homeostasis. The levels of iron in isolated cytosolic and mitochondrial fractions (Figure S3F) were greater for *Fbxl5*$^{\Delta/\Delta}$ MEFs than for *Fbxl5*$^{+/+}$ MEFs (Figure 3E), suggesting that the accumulated IRPs promote iron loading in the cytosol and mitochondria, leading to oxidative stress, in the former cells. Thus, collectively, our observations suggested that the abundance and activity of IRPs are increased in a manner independent of iron conditions, leading to increased oxidative stress and embryonic death as a result of iron overload, in FBXL5-deficient mice.

Fbxl5$^{-/-}$*Irp2*$^{-/-}$ Mice Develop Normally

To test our hypothesis that IRP accumulation is responsible for the early embryonic death of *Fbxl5*$^{-/-}$ mice, we examined whether additional ablation of IRP2, which dominates control of iron homeostasis in vivo (Meyron-Holtz et al., 2004b), prevented the embryonic mortality of these animals. Whereas most *Fbxl5*$^{-/-}$ mice died in utero at E8.5, *Fbxl5*$^{-/-}$*Irp2*$^{-/-}$ mice developed normally and were fertile (Figures 4A and 4B). *Fbxl5*$^{-/-}$*Irp2*$^{-/-}$ mice were macroscopically indistinguishable from wild-type littermates and grew normally (Figure 4C).

Iron metabolism in *Fbxl5*$^{-/-}$*Irp2*$^{-/-}$ mice appeared almost identical to that in *Irp2*$^{-/-}$ mice, with some exceptions. *Irp2*$^{-/-}$ mice manifest mild microcytic anemia and an abnormal distribution of iron within the body, including iron accumulation in the liver and a reduced iron level in the spleen (Cooperman et al., 2005; Galy et al., 2005). The hematocrit and serum concentration of hemoglobin were significantly reduced in *Irp2*$^{-/-}$ mice in association with a normal erythrocyte count and a lower mean cell volume (Table 1). The hematologic parameters of *Fbxl5*$^{-/-}$*Irp2*$^{-/-}$ mice were indistinguishable from those of *Irp2*$^{-/-}$ mice. However, the serum iron concentration as well as transferrin saturation were increased in *Fbxl5*$^{-/-}$*Irp2*$^{-/-}$ mice, whereas these parameters did not differ between *Irp2*$^{-/-}$ and wild-type mice (Table 1). Although the precise mechanism underlying these paradoxical increases remains unknown, these results suggest that the microcytosis in *Fbxl5*$^{-/-}$*Irp2*$^{-/-}$ mice is not attributable to systemic iron deficiency. We also measured organ nonheme iron content and found that it was increased in the liver and decreased in the spleen of *Irp2*$^{-/-}$ mice, consistent with previous observations, whereas the liver iron content of *Fbxl5*$^{-/-}$*Irp2*$^{-/-}$ mice was significantly decreased compared with that of *Irp2*$^{-/-}$ mice (Figure 4D). Immunoblot analysis revealed that the abundance of ferroportin was not significantly changed in the liver of *Fbxl5*$^{-/-}$*Irp2*$^{-/-}$ mice (Figure S4A). The expression of the iron-storage protein ferritin was increased in the cerebrum, liver, and kidney of *Irp2*$^{-/-}$ mice (Figure 4E). However, the abundance of ferritin in the liver of *Fbxl5*$^{-/-}$*Irp2*$^{-/-}$ mice was decreased compared with that in *Irp2*$^{-/-}$ mice, mirroring the decrease in iron content. An electrophoretic mobility shift assay (EMSA) revealed that the IRE-binding activity of IRP1 in the liver of *Fbxl5*$^{-/-}$*Irp2*$^{-/-}$ mice was increased by ~20% compared with that in *Irp2*$^{-/-}$ mice (Figures S4B and S4C), which may account for the decreased ferritin level.

We generated *Fbxl5*$^{-/-}$*Irp2*$^{-/-}$ MEFs and analyzed the response of iron-related proteins in these cells to changes in iron availability. The abundance of IRP1 in *Fbxl5*$^{-/-}$*Irp2*$^{-/-}$ MEFs was increased compared with that in *Irp2*$^{-/-}$ MEFs, and this difference was associated with a slight increase in

(D) Nonheme iron content of the liver and spleen of *Fbxl5*$^{+/+}$*Irp2*$^{+/+}$ (n = 8), *Fbxl5*$^{+/+}$*Irp2*$^{-/-}$ (n = 8), *Fbxl5*$^{+/-}$*Irp2*$^{-/-}$ (n = 10), and *Fbxl5*$^{-/-}$*Irp2*$^{-/-}$ (n = 12) mice at 9–13 weeks of age. Data are mean ± SD. **p < 0.01 (Student's t test).

(E) Immunoblot analysis of extracts of the cerebrum, liver, and kidney of 11-week-old mice of the indicated genotypes with antibodies to ferritin and to Hsp90. Two animals were examined for each genotype.

(F) Primary cultured MEFs of the indicated genotypes were incubated for 16 hr in the absence or presence of FAC (100 μg/ml) or 100 μM DFO and were then subjected to immunoblot analysis with antibodies to the indicated proteins. The asterisk indicates a nonspecific band. See also Figure S4.

Table 1. Hematologic and Serum Iron Parameters of *Fbxl5*$^{-/-}$*Irp2*$^{-/-}$ Mice

Hematologic Parameters				
Parameter	*Fbxl5*$^{+/+}$*Irp2*$^{+/+}$ (n = 11)	*Fbxl5*$^{+/+}$*Irp2*$^{-/-}$ (n = 8)	*Fbxl5*$^{+/-}$*Irp2*$^{-/-}$ (n = 11)	*Fbxl5*$^{-/-}$*Irp2*$^{-/-}$ (n = 15)
RBC count ($10^4/\mu l$)	1000 ± 37.8	952 ± 60.1	998 ± 55.4	985 ± 40.0
MCV (fl)	52.4 ± 0.6	49.3 ± 0.7[a]	48.9 ± 1.1[a]	48.7 ± 1.0[a]
Hematocrit (%)	52.4 ± 2.2	47.0 ± 3.2[a]	48.6 ± 2.5[a]	48.0 ± 1.9[a]
Serum hemoglobin (g/dl)	15.9 ± 0.7	13.7 ± 0.9[a]	14.3 ± 0.7[a]	14.0 ± 0.5[a]
MCH (pg)	15.9 ± 0.2	14.4 ± 0.4[a]	14.3 ± 0.5[a]	14.2 ± 0.3[a]
MCHC (g/dl)	30.3 ± 0.3	29.3 ± 0.5[a]	29.3 ± 0.5[a]	29.2 ± 0.5[a]
Serum Iron Parameters				
Parameter	*Fbxl5*$^{+/+}$*Irp2*$^{+/+}$ (n = 6)	*Fbxl5*$^{+/+}$*Irp2*$^{-/-}$ (n = 6)	*Fbxl5*$^{+/-}$*Irp2*$^{-/-}$ (n = 6)	*Fbxl5*$^{-/-}$*Irp2*$^{-/-}$ (n = 8)
TIBC (μg/dl)	366 ± 26. 4	359 ± 44.4	398 ± 36.9	334 ± 36.6
Iron (μg/dl)	150 ± 33.1	152 ± 32.6	163 ± 30.7	209 ± 33.5[a]
Transferrin saturation (%)	41.4 ± 11.1	42.5 ± 8.8	41.0 ± 8.8	63.9 ± 15.2[a]

Data are mean ± SD for the indicated numbers of 9- to 13-week-old mice. Transferrin saturation was calculated from measured serum iron and TIBC. RBC, red blood cell; MCV, mean cell volume; MCH, mean corpuscular hemoglobin; MCHC, mean corpuscular hemoglobin concentration; TIBC, total iron-binding capacity.

[a] $p < 0.01$ versus *Fbxl5*$^{+/+}$*Irp2*$^{+/+}$ mice (Student's t test).

TfR1 expression under iron-replete conditions (Figure 4F). These observations suggested that IRP1 activity was slightly increased in *Fbxl5*$^{-/-}$*Irp2*$^{-/-}$ mice. Thus, we concluded that the increased activity of IRP1 in *Fbxl5*$^{-/-}$*Irp2*$^{-/-}$ mice attenuated the increased hepatic levels of iron and ferritin apparent in *Irp2*$^{-/-}$ mice.

Liver-Specific Ablation of *Fbxl5*

To study the function of FBXL5 in adult mouse tissues, we next examined the consequences of FBXL5 deficiency in the liver, which plays a central role in systemic iron homeostasis. To ablate *Fbxl5* in the liver, we crossed *Fbxl5*$^{F/F}$ mice with mice harboring a Cre transgene under the control of the promoter for the albumin gene (*Alb*-Cre mice). We confirmed that almost all floxed alleles were inactivated by Cre recombinase in the liver of *Alb*-Cre/*Fbxl5*$^{F/F}$ mice, as revealed by a corresponding decrease in the amount of FBXL5 mRNA (Figure S5A). *Alb*-Cre/*Fbxl5*$^{F/F}$ mice were viable, but the liver of these animals was lighter in color compared with that of their *Alb*-Cre/*Fbxl5*$^{F/+}$ littermates (Figure 5A). Histological analysis revealed that the nuclei of cells in the liver of *Alb*-Cre/*Fbxl5*$^{F/F}$ mice remained centrally located, whereas the corresponding cytoplasm was only weakly eosinophilic and contained numerous microvesicular vacuoles (Figures 5B and 5C). Lobular infiltration of inflammatory cells such as lymphocytes and neutrophils was also observed in the liver of *Alb*-Cre/*Fbxl5*$^{F/F}$ mice (Figure 5D), indicative of hepatic inflammation. However, serum chemistry parameters associated with liver damage did not differ between the mutant and control mice under normal fed conditions (Table S1), indicating that the hepatic inflammation in the mutant animals is mild. Oil red O staining revealed deposition of multiple small lipid droplets with an undisplaced nucleus in liver cells of the mutant mice (Figures 5E and 5F), a characteristic of liver damage associated with impaired mitochondrial function (Burt, 2001). Consistent with mitochondrial dysfunction, ATP levels of *Fbxl5*$^{\Delta/\Delta}$ MEFs under basal conditions were reduced compared with those of *Fbxl5*$^{+/+}$ MEFs, and this reduction was further enhanced under high-iron conditions (Figure S5B). Moreover, electron microscopy revealed mitochondriopathy associated with small lipid droplets in FBXL5-deficient hepatocytes; the mitochondria were swollen, with a hypodense matrix suggestive of mitochondrial injury (Figures 5G–5J).

We next examined iron metabolism in *Alb*-Cre/*Fbxl5*$^{F/F}$ mice. DAB-enhanced Perls and Turnbull staining revealed the accumulation of ferrous iron in hepatocytes of *Alb*-Cre/*Fbxl5*$^{F/F}$ mice (Figures 5K–5N). Immunoblot analysis showed that IRP2 also accumulated in the liver of these mice (Figure 5O). The abundance of IRP1 was also increased in the liver of *Alb*-Cre/*Fbxl5*$^{F/F}$ mice, but the extent of this change was much less pronounced than was that observed in *Fbxl5*$^{\Delta/\Delta}$ MEFs—probably because the iron-sulfur cluster of IRP1 is readily destabilized by exposure to oxygen in cultured cells, leading to conversion of holo-IRP1 to the IRE-binding, apo-IRP1 form. Given the predominance of holo-IRP1 and the conversion of only a small fraction of this form to apo-IRP1 in mouse tissues (Meyron-Holtz et al., 2004a), the amount of apo-IRP1 in the liver of *Alb*-Cre/*Fbxl5*$^{F/F}$ mice may be masked by the more abundant holo-IRP1, which is not degraded by FBXL5 (Salahudeen et al., 2009; Vashisht et al., 2009). The upregulation of IRP2 in the liver of *Alb*-Cre/*Fbxl5*$^{F/F}$ mice was also associated with increased TfR1 expression (Figure 5O) and iron accumulation specifically in the liver (Figure 5P). The abundance of ferritin in the liver of *Alb*-Cre/*Fbxl5*$^{F/F}$ mice was paradoxically also increased despite the accumulation of IRP2 (Figure 5O). The amount of mRNA for the L chain of ferritin in the liver was greater for *Alb*-Cre/*Fbxl5*$^{F/F}$ mice than for *Fbxl5*$^{F/F}$ littermates, and this increase was greatly enhanced under conditions of oxidative stress induced by feeding the animals a high-iron diet (Figure S5C). Given that iron loss induces degradation of ferritin by the proteasome (De Domenico et al., 2006), both transcriptional and posttranslational mechanisms may contribute to upregulation of ferritin that dominates over IRP-mediated translational suppression of ferritin mRNA in the liver of *Alb*-Cre/*Fbxl5*$^{F/F}$ mice.

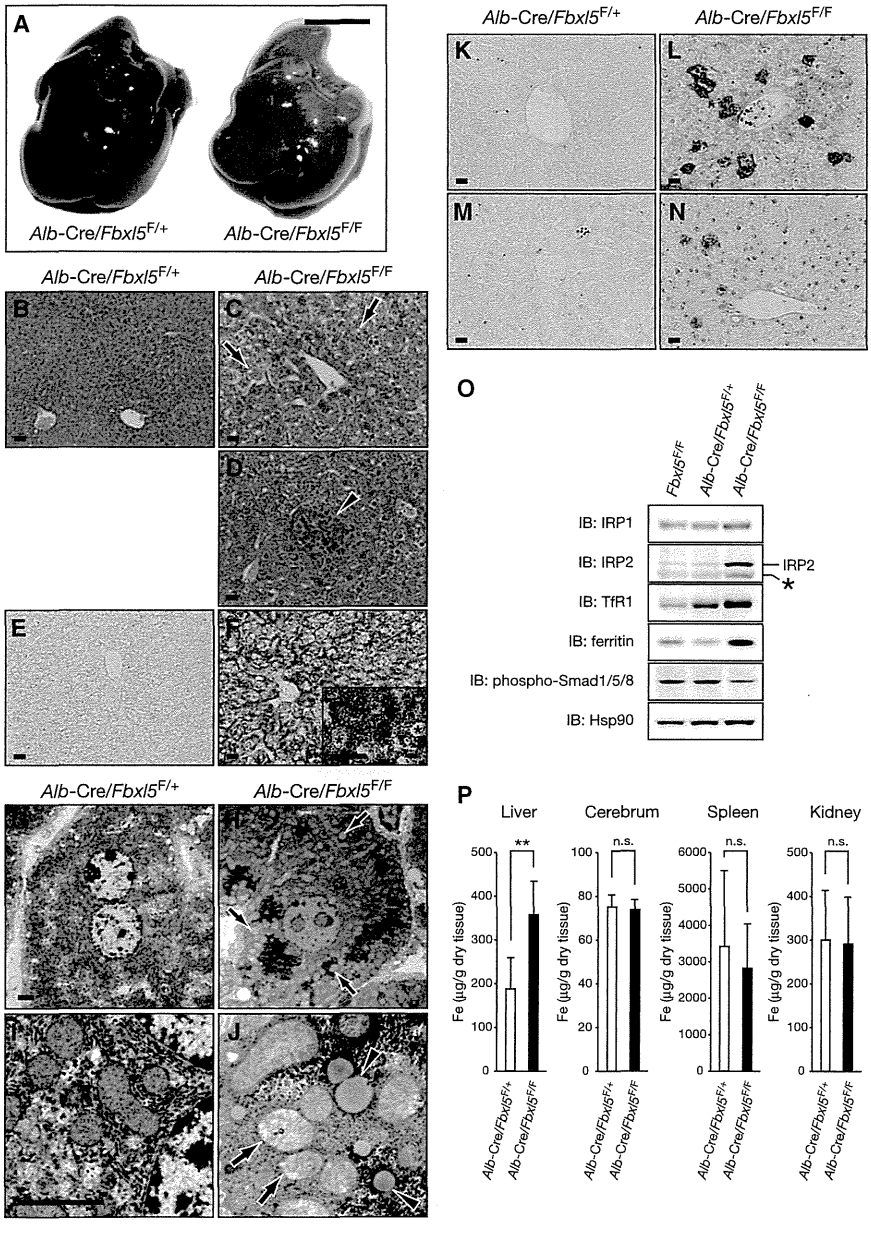

Figure 5. Hepatocyte-Specific Ablation of *Fbxl5* Results in Iron Accumulation and Steatohepatitis

(A) Gross appearance of the liver of *Alb*-Cre/*Fbxl5*$^{F/+}$ and *Alb*-Cre/*Fbxl5*$^{F/F}$ mouse littermates at 32 weeks of age. Scale bar, 10 mm.

(B–F) Histological analysis of the liver of 16- to 32-week-old *Alb*-Cre/*Fbxl5*$^{F/F}$ mice (C, D, and F) compared with that of control *Alb*-Cre/*Fbxl5*$^{F/+}$ littermates (B and E). (B–D) Hematoxylin and eosin staining. Arrows indicate numerous microvesicular vacuoles, and the arrowhead indicates lobular infiltration of inflammatory cells. (E and F) Oil red O staining. The inset in (F) shows a corresponding higher-magnification view. Asterisks indicate cell nuclei. Scale bars, 20 μm.

(G–J) Electron microscopy of the liver of 12-week-old *Alb*-Cre/*Fbxl5*$^{F/F}$ mice (H and J) compared with that of control *Alb*-Cre/*Fbxl5*$^{F/+}$ littermates (G and I). Arrows indicate numerous pale and swollen mitochondria, and the arrowheads indicate numerous lipid droplets. Scale bars, 2 μm.

(K–N) DAB-enhanced Perls staining (K and L) and DAB-enhanced Turnbull staining (M and N) of the liver of 16- to 32-week-old *Alb*-Cre/*Fbxl5*$^{F/F}$ mice (L and N) compared with that of control *Alb*-Cre/*Fbxl5*$^{F/+}$ littermates (K and M). Scale bars, 20 μm.

(O) Immunoblot analysis of liver extracts from 15-week-old mice of the indicated genotypes with antibodies to the indicated proteins. The asterisk indicates a nonspecific band.

(P) Nonheme iron content of the indicated organs of *Alb*-Cre/*Fbxl5*$^{F/+}$ (n = 4) and *Alb*-Cre/*Fbxl5*$^{F/F}$ (n = 8) mice at 16–32 weeks of age. Data are mean ± SD. n.s., not significant. **p < 0.01 (Student's t test). See also Figure S5 and Table S1.

Systemic Iron Overload in *Alb*-Cre/*Fbxl5*$^{F/F}$ Mice

We next asked how liver-specific deletion of *Fbxl5* affects systemic iron homeostasis. Serum iron levels (Figure 6A) as well as transferrin saturation (Figure 6B) were significantly increased in *Alb*-Cre/*Fbxl5*$^{F/F}$ mice, whereas hematologic parameters were not changed (Table S1). These results suggested that, inappropriately for their overall iron status, these mice might express low levels of hepcidin, the negative regulator of iron transport into plasma. The abundance of hepcidin mRNA in the liver was indeed significantly smaller for *Alb*-Cre/*Fbxl5*$^{F/F}$ mice than for *Fbxl5*$^{F/F}$ littermates (Figure 6C), and such a difference was also apparent when hepcidin gene expression was increased by feeding the animals a high-iron diet.

To elucidate the mechanism underlying the downregulation of hepcidin mRNA in the liver of *Alb*-Cre/*Fbxl5*$^{F/F}$ mice, we examined bone morphogenetic protein (BMP) signaling, which is the predominant regulator of hepcidin gene transcription (Hentze et al., 2010). Whereas the hepatic abundance of Hfe2 mRNA was unaffected (Figure S6A), that of BMP6 mRNA was smaller for *Alb*-Cre/*Fbxl5*$^{F/F}$ mice than for *Fbxl5*$^{F/F}$ littermates, and this difference was also apparent when *Bmp6* expression was increased by feeding the animals a high-iron diet (Figure S6B). We also examined receptor-activated Smad phosphorylation and found that the phosphorylation level of Smad1, Smad5, and Smad8 (Smad1/5/8) was decreased in the liver of *Alb*-Cre/*Fbxl5*$^{F/F}$ mice (Figure 5O). The amounts of mRNAs for suppressors of hepcidin gene transcription such as Smad6, Smad7, and transmembrane serine protease 6 (Tmprss6) were not increased in the liver of *Alb*-Cre/*Fbxl5*$^{F/F}$ mice, but rather were paradoxically decreased (Figure S6C). Increased iron did not activate Smad7 transcription in the liver of *Alb*-Cre/*Fbxl5*$^{F/F}$ mice, likely as a result of decreased BMP signaling (Kautz et al., 2008). Collectively, these findings indicated that BMP signaling in the liver of *Alb*-Cre/*Fbxl5*$^{F/F}$ mice is decreased as a result of the reduced expression of *Bmp6*, and they suggested that the decrease in *Bmp6* expression is likely responsible for downregulation of